Oxygen isotope heterogeneity of arc magma recorded in plagioclase from the 2010 Merapi eruption (Central Java, Indonesia)

Anastassia Y. Borisova, Andrey A. Gurenko, Caroline Martel, Kalin Kouzmanov, Annick Cathala, Wendy A. Bohrson, Indyo Pratomo, Sri Sumarti

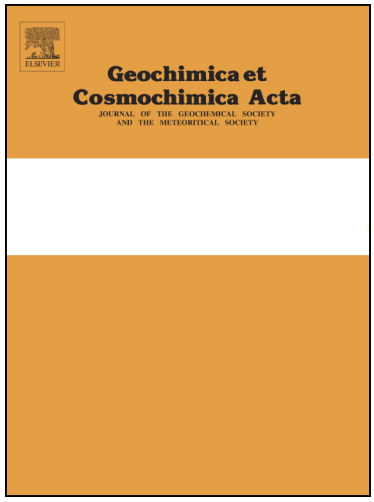

Oxygen isotope heterogeneity of arc magma recorded in plagioclase from the 2010 Merapi eruption (Central Java, Indonesia)

Anastassia Y. Borisova, Andrey A. Gurenko, Caroline Martel, Kalin Kouzmanov, Annick Cathala, Wendy A. Bohrson, Indyo Pratomo, Sri Sumarti

PII: S0016-7037(16)30350-7
DOI: http://dx.doi.org/10.1016/j.gca.2016.06.020
Reference: GCA 9816

To appear in: *Geochimica et Cosmochimica Acta*

Received Date: 7 July 2015
Accepted Date: 13 June 2016

Please cite this article as: Borisova, A.Y., Gurenko, A.A., Martel, C., Kouzmanov, K., Cathala, A., Bohrson, W.A., Pratomo, I., Sumarti, S., Oxygen isotope heterogeneity of arc magma recorded in plagioclase from the 2010 Merapi eruption (Central Java, Indonesia), *Geochimica et Cosmochimica Acta* (2016), doi: http://dx.doi.org/10.1016/j.gca.2016.06.020

Oxygen isotope heterogeneity of arc magma recorded in plagioclase from the 2010 Merapi eruption (Central Java, Indonesia)

Anastassia Y. BORISOVA[1,2*], Andrey A. GURENKO[3], Caroline MARTEL[4], Kalin KOUZMANOV[5], Annick CATHALA[1], Wendy A. BOHRSON[6], Indyo PRATOMO[7], Sri SUMARTI[8]

[1]*Géosciences Environnement Toulouse, Université de Toulouse; UPS OMP- CNRS - IRD, 14 Avenue E. Belin, 31400 Toulouse, France*

[2]*Geological Department, Lomonosov Moscow State University, Vorobievu Gory, 119899, Moscow, Russia*

[3]*Centre de Recherches Pétrographiques et Géochimiques, UMR 7358, Université de Lorraine,, 54501, Vandoeuvre-lès-Nancy, France*

[4]*Institut de Sciences de la Terre, Université d'Orléans, CNRS/INSU ISTO, UMR 7327 Orléans, France*

[5]*Department of Earth Sciences, University of Geneva, rue des Maraîchers 13, CH-1205 Geneva, Switzerland*

[6]*Department of Geological Sciences, Central Washington University, Ellensburg, WA 98926, USA*

[7]*Museum Geologi, Pusat Survei Geologi, Jln. Diponegoro No. 57, Bandung, Indonesia*

[8]*Volcano Investigation and Technology Development Institution, Yogyakarta, Indonesia*

[*]Corresponding author: E-mail: anastassia.borisova@get.obs-mip.fr;

[*]Corresponding address: Géosciences Environnement Toulouse UMR 5563, Observatoire Midi Pyrénées, 14 Avenue E. Belin, 31400 Toulouse, France; Tel: +33(0)5 61 54 26 31; Fax: +33(0)5 61 33 25 60

Keywords: Merapi, plagioclase crystals, oxygen isotopes, calc-silicate xenoliths, crustal assimilation, timescale

ABSTRACT

Chemical and isotopic compositions of magmatic crystals provide important information to distinguish between deep juvenile and crustal contributions. In this work, high-resolution multicollector secondary ion mass spectrometry data reveal strong variations of $\delta^{18}O$ values in three plagioclase crystals (800 – 1700 μm) from two representative basaltic andesite samples of the 2010 Merapi eruption (Central Java, Indonesia). The $\delta^{18}O$ values (from 4.6 to 7.9 ‰) are interpreted to reflect oxygen isotope heterogeneity in the melt composition during plagioclase growth. The lowest $\delta^{18}O$ values (4.6 – 6.6 ‰) are found in anorthite-rich cores ($An_{82–97}$), whereas higher $\delta^{18}O$ values (5.7 to 7.9 ‰) are found in anorthite-poorer zones ($An_{33–86}$), typically in crystal rims. Combining these new plagioclase $\delta^{18}O$ data with $\delta^{18}O$ of calc-silicate crustal xenoliths erupted between 1994 – 1998, the composition of glass inclusions hosted by the anorthite-rich plagioclase (An_{82-92}), available experimental data, and the results of thermodynamic modelling using the Magma Chamber Simulator code, we conclude that the abundant anorthite-rich cores crystallized from a mantle-derived hydrous basaltic to basaltic trachyandesite melt that recharged a deeper (200-600 MPa) magma storage zone, whereas lower anorthite zones crystallized at shallower levels (100-200 MPa). The oxygen isotope variations in the plagioclase are explained by a two-stage model of interaction of the hydrous, mafic mantle-derived magma (1) with old crustal rocks depleted in ^{18}O due to high temperature alteration that yielded the low $\delta^{18}O$ values in the anorthite-rich cores at deep levels (13 – 20 km), and later (2) with ^{18}O-enriched carbonate material that yielded the high $\delta^{18}O$ values in anorthite-poorer zones at shallow levels (~4.5 – 9 km). Thermodynamic modelling is consistent with ~18 wt.% assimilation of crustal calc-silicate material at 925 – 950°C and 100 – 200 MPa by the 2010 Merapi basaltic andesite magma prior to eruption. Timescales for plagioclase phenocryst growth and residence in the magmatic plumbing

system are ≤34 years. The combined data thus reveal efficient magma recharge and crustal assimilation processes that characterize the open-system magma storage and transport systems associated with the 2010 Merapi eruption.

1. INTRODUCTION

One of the major challenges in understanding arc magmatism is to identify and quantify the components that lead to the observed geochemical diversity. This information is fundamental for creating global mass transfer models and for assessing the mass of Earth materials that are fed into the mantle *via* subduction zones. Identifying source components of the near-primary, least fractionated, mafic magmas is not a simple task; moreover, such magmas are rarely erupted in convergent margin settings. More often, one has to study magmas of intermediate composition and thus to account for the added complexity of crustal magma processes, such as fractional crystallization, open-system degassing, crustal assimilation and magma mixing. Erupted lavas, which are typically aggregated at pre-eruptive conditions (e.g., Bindeman et al., 2005; Reubi and Blundy, 2009), commonly represent mixtures of crystals and melts that may have different evolutionary histories and/or sources. Investigating chemical (both elemental and isotopic) zoning in representative crystals of magmatic products is thus a viable way to augment our understanding of the variety of components that contribute to arc magma signatures (e.g., Davidson et al., 2007).

Plagioclase is a very common mineral in the Earth's crust and extraterrestrial materials (Taylor and McLennan, 1985; Papike et al., 1998; Brearley and Jones, 1998; Lange et al., 2013). Its calcic end-member, anorthite, is frequently found in cores of crystals in igneous inclusions and crustal xenoliths, and is particularly abundant in arc-related magmatic rocks

(e.g., Bindeman and Bailey, 1999; Pichavant et al., 2002; Martel et al., 2006; Chadwick et al., 2007; Plechov et al., 2008; Deegan et al., 2010; Troll et al., 2013; Borisova et al., 2013), thereby implying their importance in unravelling the early history of the subduction-related magmas. Indeed, starting from its primary source, magma constantly interacts with surrounding solid material as well as other magmas. To constrain the composition of magmatic sources and additional crustal components, it is important to document the chemical and isotopic exchange mechanisms that control magma genesis. For arc magmas interacting with carbonate crust, as seen at Merapi, the mechanisms of the crustal assimilation may be deciphered from natural samples and through experiments (Freda et al., 2008; Gaeta et al., 2009, Iacono-Marziano et al., 2008, 2009; Deegan et al., 2010; Mollo et al., 2010; Borisova et al., 2013; Jolis et al., 2013). Recent advances in *in situ* microanalytical methods (e.g., Davidson et al., 2007), thermodynamic and geochemical modelling (Zhang and Cherniak, 2010; Bohrson et al., 2014), and experimental approaches at high pressure-temperature conditions (e.g., Deegan et al., 2010; Jolis et al., 2013) make it now possible to develop novel petrogenetic models and constrain such magma-crust interaction processes and their timescales in more detail.

To test these "process-signal" relationships, we have chosen Merapi volcano (Central Java, Indonesia) due to its detailed record of crustal processes in the igneous products. Using an integrated approach, we examine here the role of both magma-crust and magma-magma interactions in the 2010 eruption of Merapi, Indonesia. In particular, *in situ* microanalytical methods often reveal larger variations of isotope ratios at a micrometer scale, as compared to the grain- and rock-scales (e.g., Davidson et al., 2007; Chadwick et al., 2007; Borisova et al., 2014; Winpenny and Maclennan, 2014); these observations prompted us to further explore isotopic and elemental information from Merapi volcano. We obtained this information from the most abundant crystalline phase, plagioclase, in the 2010 Merapi eruptive products, by

employing *in situ* oxygen isotope composition determined using multicollector secondary ion mass spectrometry (SIMS). Three representative Merapi 2010 plagioclase crystals reveal considerable intra-crystal isotopic heterogeneity. Additionally, we compare these new *in situ* plagioclase data with new grain-scale oxygen isotope analyses of several mineral fractions from representative calc-silicate xenoliths that are frequently observed in the recent Merapi volcanic products. Finally, to more fully constrain the petrogenetic processes that produced the 2010 Merapi plagioclases, we performed thermodynamic modelling utilizing the new the Magma Chamber Simulator code (Bohrson et al., 2014) and anorthite-rich plagioclase-hosted melt inclusions.

2. GEOLOGICAL BACKGROUND

Merapi stratovolcano is located 25–30 km north of the city of Yogyakarta, Indonesia (Fig. 1). The volcano is composed mainly of basaltic-andesite tephra, pyroclastic flows, lava, and lahar deposits. Since the 19th century, Merapi has erupted every 4 – 6 years, with most of these eruptions having explosivity indices ≤VEI 2, although moderate VEI 3 (1832, 1849, 1930, 1961) to large VEI 4 (1822, 1872) eruptions have also occurred (Costa et al., 2013). However, in late October and early November of 2010, Merapi changed its eruptive style, producing its most powerful, explosive and voluminous eruption in the last 100 years. This eruption likely marked a change in Merapi's activity towards more explosive behavior (Surono et al., 2012).

Numerous methods (melt inclusion study, *in situ* mineral and glass chemistry analyses, ash leaching, bulk rock analyses and geochemical modelling) have been applied to constrain composition of the 2010 pre-eruptive melts and bulk syn-eruptive fluid (Borisova et al., 2013; Costa et al., 2013; Preece et al., 2014). The work of Borisova et al. (2013) suggests that the

paroxysmal eruption was produced by pre-eruptive saturation of basaltic andesite magma with a hybrid, aqueous carbonic NaCl-HCl-rich fluid that generated elevated partial pressures of crustally-derived CO_2 at conditions of about 200 MPa. Several chemical and physical parameters suggest that the magma assimilated calc-silicate xenoliths issued from the surrounding carbonate-bearing crust (Javanese limestone, Borisova et al., 2013; Troll et al., 2013). Recent field expedition of A.Y. Borisova, I. Pratomo and S. Sumarti in 2015 confirmed the occurrence of calc-silicate xenoliths in the 2010 eruptive products. Although no fragments of metamorphosed calc-silicate minerals had been previously found in the eruptive products (Borisova et al., 2013), the mineralogy, mineral and glass chemistry, and the bulk-rock Sr isotope composition of the 2010 Merapi basaltic andesite lavas suggest that the pre-eruptive magma might have assimilated from 15 to 40 wt.% of the shallow-level carbonate-rich silicate crustal material. If this estimate is correct, then such a process could result in introduction of an additional 0.19 to 2.1 Mt of CO_2 into the shallow-level (~6 km depth) magma chamber, thereby explaining why plagioclase crystals from the 2010 Merapi pyroclastic flow and tephra have highly variable compositions (from An_{45} to An_{97}) (Borisova et al., 2013). In this context, the bulk-rock ^{18}O composition of ash samples, which is as high as 6.9‰ $\delta^{18}O$, was explained by complete digestion of the 1998 and 2006-type calc-silicate xenoliths preceding the 2010 eruption (Borisova et al., 2013; Troll et al., 2013). Borisova et al. (2013) demonstrated that the crustal assimilation process proceeded through three major steps: (1) contact metamorphism of the Javanese limestone and formation of calc-silicate xenoliths of the 1998 and 2006 type; (2) bulk assimilation of the calc-silicate xenoliths through complete digestion, melting/dissolution and generation of the calcic melts representing the Crustal Assimilant; (3) effective binary chemical and physical mixing between hydrous K-rich and the Crustal Assimilant end-member melts that bear both signatures (i.e., magmatic and crustal), accompanied by fractional crystallization of

phenocrysts. Previous data on oxygen isotope compositions of multigrain plagioclase fractions from two pyroclastic flow and tephra samples issued from the Merapi 2010 eruption (6.5 ‰ of $\delta^{18}O$; Borisova et al., 2013) could have indicated isotopic homogeneity of plagioclases, but at that time, no intra-crystal data for oxygen isotopes were available for Merapi.

3. MATERIALS AND ANALYTICAL TECHNIQUES

3.1. Natural and reference materials

The studied plagioclase crystals are representative of the Merapi pyroclastic flows deposited in October 2010 (M2010GR and M2010PF; Fig. 2). The sampling location and detailed descriptions of the 2010 Merapi plagioclases are given in Borisova et al. (2013). For example, figure 4 of Borisova et al. (2013) represents chemical profiling of one of the plagioclase phenocrysts typical of the 2010 pyroclastic flow (M2010PF). Previous data from the 2010 ashes obtained using Energy Dispersive X-ray Spectroscopy (using SEM, JEOL JSM-6360 LV, see below) revealed abundant plagioclase fragments with contents reaching 16 % of the analyzed sample surface made up of anorthite and up to 55% of the sample surface made up of less calcic plagioclases.

The investigated calc-silicate xenoliths are from the 1994 and 1998 eruptions of Merapi, and further information on these samples is listed in Table A1. Samples M94-CS-104 and M94-CS-106 are from the 1994 small-volume Merapi block-and-ash flows. Samples MXCS-1 and MXCS-4 are from the 1998 block-and-ash flows. The sampling location and

detailed mineralogical and chemical descriptions are given in Chadwick et al. (2007) and are shown in Deegan et al. (2010).

Five natural homogeneous plagioclase crystals of sub-mm to several mm size and of high clarity were used as reference materials to analyze *in situ* oxygen isotope composition by SIMS. The samples are: Std 1 - Amelia albite (Amelia County, VA, $An_{0.32}$); Std 2 - Mitchell oligoclase (Mitchell County, $An_{23.6}$); Std 3 - labradorite (Beaver Bay, Minnesota, $An_{61.1}$); Std 5 - ED09An2 labradorite ($An_{55.0}$) and Std 6 - anorthite (Zheltovsky volcano, Kamchatka, CI 114, $An_{90.3}$).

3.2. Scanning Electron Microscope (SEM) and Electron Microprobe analysis (EMPA)

Major element analyses of minerals and glasses from the pyroclastic flows and xenoliths were performed at the Géosciences Environnement Toulouse (GET, Toulouse, France) laboratory using a scanning electron microscope (SEM) JEOL JSM-6360 LV with energy-dispersive X-ray spectroscopy (EDS), coupled with the automatic particle analyzer by the program "Esprit". The main mineral phases (anorthite, grossular, titanomagnetite, wollastonite) in the Merapi calc-silicate xenoliths (Table A1), were first separated into different mineral fractions (for laser fluorination analysis) and have been identified by EDS microprobe technique. Major, minor and volatile element compositions of the 2010 Merapi plagioclase crystals and glass inclusions and the five reference plagioclases were analyzed using both the CAMECA SX-50 and CAMECA SX-Five microprobes at the GET laboratory and the Centre de Microcaractérisation Raimond Castaing (Toulouse, France), respectively. The analytical procedure was previously described in Borisova et al. (2013). Electron beam of 15 kV accelerating voltage, and of 10 – 20 nA current and < 1µm size was focused on the sample to

give analytical lateral resolution of ≤ 2 μm^2. The following synthetic and natural standards were used for calibration: albite (Na), corundum (Al), wollastonite (Si, Ca), sanidine (K), $MnTiO_3$ (Mn, Ti), hematite (Fe), and MgO (Mg), $SrSO_4$ (S), topaz (F), tugtupite (Cl), Ni alloy (Ni), Cr_2O_3 (Cr). Element and background counting times for all analyzed elements were 10 and 5 s, respectively. The detection limit for Fe (1400 ppm) correspond to 0.18 wt.% FeO. Most MgO contents in the analyzed plagioclases are close to the MgO detection limit of 0.06 wt.% (577 ppm of Mg), and, therefore, these data are not discussed. Typical uncertainties of the FeO contents in the plagioclases were 0.17 wt.% at the above mentioned analytical conditions. The silicate reference materials of Jarosewich et al. (1980) were analyzed as unknown samples to additionally monitor analysis quality and to control precision for the major and minor (e.g., FeO in plagioclase) element analyses to be within the limit of the analytical uncertainty (related to the count statistics). The reproducibility (better than 0.17 wt.%) for the EMPA analyses estimated based on repetitive measurements of the MPI-DING series reference glasses (Jochum et al., 2006) is within the limit of the analytical uncertainty for major elements.

3.3. Laser fluorination of natural and reference materials

Single grain laser fluorination oxygen isotope data were collected in the stable isotope laboratory of the University of Oregon (Eugene, Oregon, USA; Bindeman, 2008). Due to the large size of the five individual crystals of plagioclases used as standards (Stds 1, 2, 3, 5, 6) in the present study and the large amount of the xenolith crystal fractions, these crystals were characterized for oxygen isotopic composition by laser fluorination relying on the single 1-mg-chunks of the material. Pure mineral separates of the reference plagioclases as well as several fractions of pure mineral (wollastonite, titanomagnetite) and the mineral assemblages

from the 1994 – 1998 Merapi calc-silicate xenoliths were analyzed by heating with an infrared laser (9.6 μm, CO_2) in the presence of purified BrF_5 to release oxygen for each sample. The generated O_2 gas was purified in a series of cryogenic traps held at liquid nitrogen temperature, and then a mercury diffusion pump was used to remove any remaining traces of fluorine gas. Oxygen was converted to CO_2 gas by reacting with red-hot graphite-Pt converter, the yields were measured, and CO_2 was analyzed in a dual inlet mode on MAT 253 mass spectrometer. Two garnet standards UOG ($\delta^{18}O$ 6.52 ‰, University of Oregon garnet from Gore Mt, NY, USA) and UWG-2 ($\delta^{18}O$ 5.80‰, Valley et al., 1995) bracketed the samples during the analytical session. Day-to-day $\delta^{18}O$ variability of standards ranged from 0.1 to 0.3 ‰ lighter than their reference values, and the measurements of unknowns were adjusted accordingly. The precision on standards is better than 0.08 of 1σ standard deviation.

3.4. Secondary ion mass spectrometry (SIMS)

The $^{18}O/^{16}O$ ratios in the unknown 2010 Merapi plagioclase crystals and five reference plagioclases (Stds 1, 2, 3, 5, 6) were measured using a CAMECA IMS 1280 HR (high resolution) ion microprobe at the Centre de Recherche Pétrographiques et Géochimiques (CRPG, Nancy, France). The investigated plagioclase crystals (also analyzed for major element composition by electron microprobe) and fragments of four reference plagioclase crystals (Stds 1, 2, 3, 5) were mounted together in the center of 1 inch-size diameter sections (Fig. A1). To minimize possible additional analytical uncertainty related to more than 1 μm relief difference between the embedded crystals and epoxy resin (Kita et al., 2009), the crystals were placed together into epoxy resin in the central part of a Cu-Zn alloy (brass) ring.

The mounts were hardened, ground and thereafter polished using 6 to 1 μm diamond films to ensure an even sample surface.

The gold coated samples were sputtered with 10 kV Cs^+ primary beam of 6 to 8 nA current focused to ~15 – 20 μm spot. A normal-incidence electron flood gun was used for sample charge compensation. The energy slit was centered and opened to 50 eV. After pre-sputtering during 60 s, secondary $^{16}O^-$ and $^{18}O^-$ ions were accelerated at 10 kV and analyzed at mass resolving power ($M/\Delta M$) of 2500 using a circular focusing mode and a transfer optic field of view of ~150 μm. An automated routine to center consequently the secondary ion beam in the field and then in the contrast apertures was applied at the beginning of each measurement. The $^{18}O/^{16}O$ isotopic ratios were analyzed in multi-collector mode using two off-axis Faraday cups, L'2 and H1, for simultaneous counting of $^{16}O^-$ and $^{18}O^-$ ion intensities, respectively. The gain and offset of the Faraday cups was calibrated daily, using the CAMECA built-in amplifier calibration routine. The registered raw $^{16}O^-$ and $^{18}O^-$ signals were then corrected for the Faraday cup backgrounds measured during pre-sputtering time of the each run. Typical ion intensities of ~2 to 3×10^9 and ~4 to 6×10^6 counts per second (cps) have been obtained on the ^{16}O and ^{18}O masses, respectively. The in-run uncertainty is better than ±0.1‰ (1σ standard deviation) reached after 150 s analysis signal (30 cycles each of 5 s peak counting time).

3.5. SIMS data reduction

It was demonstrated that instrumental mass fractionation (IMF, also called "mass bias") for plagioclase is related to anorthite content (Valley and Kita, 2009; Winpenny and Maclennan,

2014). Thus, we used four well-characterized reference plagioclases ($An_{0.32}$, $An_{23.56}$, $An_{55.03}$, and $An_{61.09}$) to quantify IMF in the unknown plagioclase crystals. As stated above, the reference plagioclases were first analyzed for oxygen isotopes by laser fluorination technique and then multiple fragments of crystals from the same sample were examined for inter- and intra-crystal oxygen isotope homogeneity by SIMS.

To correct for IMF and also to account for possible instrumental drift, every 15 to 20 spots analyzed in the unknown plagioclase samples were bracketed by 3 to 5 spots on each of the four reference plagioclases. The instrumental mass fractionation was calculated using the $\delta^{18}O_{SMOW}$ (relative to Vienna standard mean ocean water, V-SMOW) "true" values of the reference plagioclase material (RM):

$$\Delta^{18}O_{IMF(RM)} = \delta^{18}O_{SIMS\ (RM)} - \delta^{18}O_{true\ (RM)} \quad (1),$$

where $\Delta^{18}O_{IMF(RM)}$ is the IMF measured on the reference plagioclases, $\delta^{18}O_{true\ (RM)}$ is the "true" $\delta^{18}O$ value of the reference material measured by laser fluorination and $\delta^{18}O_{SIMS\ (RM)}$ is its oxygen isotope composition measured by SIMS. The used delta notation was derived from $\delta^{18}O = [(^{18}O/^{16}O - {}^{18}O/^{16}O_{SMOW})/^{18}O/^{16}O_{SMOW}] \times 1000$ basic equation, where $^{18}O/^{16}O_{SMOW} = 0.0020052 \pm 0.00000043$ (Baertschi, 1976). The determined $\Delta^{18}O_{IMF(RM)}$ values are given in Table 1. The analyzed natural samples of interest (A, derived from "analyzed") were then corrected for IMF ($\Delta^{18}O_{IMF(RM)}$) as following:

$$\delta^{18}O_{corrected\ (A)} = \delta^{18}O_{SIMS\ (A)} - \Delta^{18}O_{IMF(RM)} \quad (2),$$

where $\delta^{18}O_{corrected(A)}$ is the corrected value of the $\delta^{18}O$ in the analyzed sample, $\delta^{18}O_{SIMS\ (A)}$ is the oxygen isotope composition measured in the sample by SIMS.

It is well-known that IMF can vary as a function of physical or chemical properties of a target material (matrix effect). In particular, oxygen isotope fractionation defined for

basaltic glasses shows significant correlations with SiO_2, FeO and CaO contents and (Na+K)/Al atomic ratios of the glasses, whose slope and intercept can vary between different analytical sessions as a result of particular instrument setting and analytical conditions (Gurenko et al., 2001). As shown later by Valley and Kita (2009) and Winpenny and Maclennan (2014), measured and uncorrected for IMF $\delta^{18}O_{SIMS}$ values can be several per mil off the plagioclase true values. Thus the IMF ($\Delta^{18}O_{IMF}$) must always be taken into account and it was calculated as:

$$\Delta^{18}O_{IMF} \approx 10^3 \ln\left[\left({}^{18}O/{}^{16}O_{SIMS}\right)/\left({}^{18}O/{}^{16}O_{true}\right)\right] \quad (3)$$

where ${}^{18}O/{}^{16}O_{SIMS}$ is oxygen isotope ratio measured by SIMS and ${}^{18}O/{}^{16}O_{true}$ is true isotope ratio.

We observe the following linear correlations of average $\Delta^{18}O_{IMF(RM)}$ estimated (based on Eqn. 1) in the four reference plagioclases ranging in composition from almost pure albite through labradorite, as a function of anorthite (An) content (Fig. A2):

$$\Delta^{18}O_{IMF(RM)} = a\left[\text{An, mol.\%}\right]_{(RM)} + b \quad (4)$$

where a are three values from 0.0415 to 0.0451 and b ranges from -13.746 to -13.425 in correlation lines built using the fours reference plagioclases in the each of three analytical data subsets (i.e., the subsets including each of three natural plagioclase samples profiles) performed during the first analytical session (26 – 29/01/2015). It should be noticed that the slopes a (~0.04) of the linear correlations defining average $\Delta^{18}O_{IMF(RM)}$ in the analytical session (Fig. A2) are similar to the coefficient range reported by Winpenny and Maclennan (2014). The regression coefficient R^2 varies from 0.996 (for M2010PF-b1 AB), 0.981 (for M2010PF-a AB) to 0.994 (for M2010GR-a AB) in the corresponding analytical subsets in the

first analytical session. The $\Delta^{18}O_{IMF(RM)}$ is average instrumental fractionation in the reference plagioclase typical for the given analytical subset, and $[An, mol.\%]_{(RM)}$ is average anorthite content measured by EMPA in the given reference plagioclase. Because no instrumental drift has been observed during analytical session, the natural plagioclase composition was corrected using the average $\Delta^{18}O_{IMF(RM)}$ characteristic for a given analytical session.

Assuming that the instrumental mass fractionation of the reference plagioclases ($\Delta^{18}O_{IMF(RM)}$) corresponds to that of the analyzed plagioclase ($\Delta^{18}O_{IMF(A)}$) for the given analytical data subset, the final equation is the following:

$$\delta^{18}O_{corrected\ (A)} = \delta^{18}O_{SIMS\ (A)} - \Delta^{18}O_{IMF(A)} \quad (5)$$

where $\Delta^{18}O_{IMF(A)}$ is calculated according to Eqn. (4) for the given anorthite content of each particular point of the 2010 Merapi plagioclase profile (Table A2). The final value of $\delta^{18}O_{corrected\ (A)}$ (in Eqn. 5) is calculated as average from the minimal and maximal values of the anorthite contents (attributed to each particular point of the SIMS profile) and applying equation (4).

3.6. SIMS analysis error propagation and accuracy

The uncertainty of an individual $\delta^{18}O$ measurement u(IM) (‰) can be defined as:

$$u^2(\mathrm{IM}) = \sigma^2(\mathrm{signal})\ /n + u^2(\mathrm{IMF}) + u^2(\mathrm{RM}) \quad (6),$$

where σ(signal) is the standard deviation (usually ±0.2 – 0.5‰, 1σ) of the measured $\delta^{18}O$ values over n cycles (n = 30); u(IMF) is the uncertainty of instrumental mass fractionation

defined as the a deviation of IMF values obtained on the each particular reference plagioclase (Stds 1, 2, 3, 5) from the regression line (Eqn. 4) and calculated as:

$$\sigma_y^2 = \frac{1}{N-2}\sum_{i=1}^{N}(y_i - ax_i - b)^2 \quad (7),$$

where a and b are constants in the linear regression (Eqn. 4) and N is a number of individual measurements (usually varying between 0.1 – 0.5‰); and u^2(RM) is the uncertainty of the δ^{18}O "true" values of the reference materials used for calibration (assigned to 0.1‰, 1σ, that corresponds to a common analytical uncertainty of laser fluorination). On average, the uncertainty of the individual δ^{18}O measurement u(IM) was thus obtained to be from 0.11‰ to 0.22‰ (1σ error) for different plagioclase crystals.

Whereas the estimated 1σ error of the δ^{18}O values of plagioclase zones varies from 0.11 – 0.22‰, the accuracy of the anorthite-rich plagioclase measurements has been estimated differently following the method of Winpenny and Maclennan (2014). The accuracy was assessed by preparing a separate epoxy mount (e.g., Fig. A1) containing multiple grains of five reference plagioclases (Stds 1, 2, 3, 5, 6) and considering analytical data obtained during second SIMS session (08 – 09/05/2015), where all five standards have been analyzed. Similarly to Fig. A2, we observe a linear correlation of average $\Delta^{18}O_{IMF(RM)}$ as a function of anorthite (An) content with the regression coefficient R^2 of 0.945 (Fig. A3, Table A3, Electronic Appendix).

$$\Delta^{18}O_{IMF(RM)} = a'\left[\text{An, mol.\%}\right]_{(RM)} + b' \quad (8),$$

where a' is 0.048 and b' is -4.835 in correlation line plotted for fours reference plagioclase standards (Stds 1, 2, 3, 5) which were used for determinations of the IMF versus anorthite relationship during the first analytical session. From this line, obtained during the second

SIMS session, the modelled $\delta^{18}O$ value for the anorthite standard (Std 6, Table A3) was then calculated using its known anorthite content, which allowed us to calculate a mismatch in $\delta^{18}O$ to that known from laser fluorination analysis. The mismatch for the anorthite plagioclase measurement ($An_{90.3}$) is 0.34 ‰ and therefore this value was taken as the accuracy of the anorthite-rich plagioclase measurements by SIMS.

4. RESULTS

In the following sections, we describe the results of our investigation of the three selected plagioclase phenocrysts, focusing on their compositional variations and considering also new isotopic data on the 1994 – 1998 Merapi calc-silicate xenolith fractions. We also describe the thermodynamic modelling performed using the Magma Chamber Simulator.

4.1. 2010 Merapi plagioclases

4.1.1. M2010GR-a plagioclase crystal

Figure 3 illustrates anorthite (An), FeO and $\delta^{18}O$ zonations in plagioclase M2010GR-a along the profile AB (Table A2, Electronic Appendix). The central zone of the crystal hosts melt inclusions visible in the optical microscope image (Fig. 3a). Figure 3(b-c) shows that the crystal is zoned with a ~1400µm-wide anorthite-rich core ($An_{89–93}$, FeO = 0.4 – 0.8 wt.%) with a low An ($An_{51–83}$) domain at its centre. In the $\delta^{18}O$ profile (Fig. 3d), zonation is also apparent. Whereas the central zone is low in An ($An_{51–83}$), it is characterized by higher $\delta^{18}O$ (6.4 – 7.2 ‰) than normal mid-ocean ridge basalt ($\delta^{18}O$ ~ 5.6 ± 0.2‰, Eiler et al., 2000). Such features may be related to a healing of this central zone by An-poor plagioclase after a resorption event due to dissolution prior to renewed crystal growth (e.g., Singer et al., 1993 and references therein). The lowest $\delta^{18}O$ value (4.1‰) coincides with the interior melt inclusion-bearing anorthite-rich domain (Fig. 3), and thus, this value is excluded from the following consideration. The anorthite-rich core ($An_{89–93}$) generally exhibits low $\delta^{18}O$ (4.6 – 6.4 ‰). The lowest values down to 4.6 ‰ are below the range recorded in the recent Javanese mantle-derived rocks (5.6 – 6.1 ‰, e.g., Harmon and Gerbe, 1992). The rim zone, which is low in An (down to An_{40}), contains 0.4 – 0.9 wt.% FeO, being similar to the values recorded in the anorthite-rich core, but shows relatively high $\delta^{18}O$ (6.0 – 7.3‰) values.

4.1.2. M2010PF-a plagioclase crystal

Figure 4 shows plagioclase M2010PF-a. Optical and electron microscope (BSE) images and phenocryst zonations were analyzed along the profile AB with respect to anorthite, FeO contents and $\delta^{18}O$ (Table A2, Electronic Appendix). The crystal is zoned, with a broad

anorthite-rich core of ~1700-μm-size ($An_{89–97}$, FeO = 0.2 to 0.8 wt.%) (Fig. 4c). The core is surrounded by an An-poorer rim of ~250 μm width ($An_{61–86}$) with variable $\delta^{18}O$ (5.7 – 6.9 ‰). The rim is similar to the core in respect of FeO contents (0.4 – 0.9 wt.%). In the $\delta^{18}O$ profile (Fig. 4d), random variations of 1.5 to 2 ‰ are apparent in the core of the crystal. Notably, the anorthite core is associated with the lower values of $\delta^{18}O$ (5.0 to 6.5 ‰).

4.1.3. M2010PF-b1 plagioclase crystal

The elemental and oxygen isotope compositions of plagioclase phenocryst M2010PF-b1 were measured along the profile AB (Fig. 5). The corresponding point-to-point analytical data are given in Table A2 (Electronic Appendix). This crystal is strongly zoned, with the core containing two 200 μm-wide anorthite-rich ($An_{88–93}$) domains surrounding a central, ~170 μm-wide low anorthite (An_{44-80}) area (Fig. 5c). The anorthite-rich domains have FeO = 0.3 – 0.8 wt.% contents. In the $\delta^{18}O$ profile, random variations are apparent (Fig. 5d), and the broad anorthite-rich domains ($An_{88–93}$ and $An_{88–91}$) show $\delta^{18}O$ of 5.0 – 6.6 ‰. The lowest $\delta^{18}O$ values, down to 5.0 ‰, are below the range recorded in recent Javanese mantle-derived rocks (5.6 – 6.1 ‰, e.g., Harmon and Gerbe, 1992). The outer rims are relatively low in anorthite ($An_{33–79}$) and vary in $\delta^{18}O$ (5.8 – 7.9 ‰), but have FeO = 0.4 – 0.6 wt.% contents that are comparable to those of the core.

4.2. 1994 – 1998 Merapi calc-silicate xenolith fractions

Oxygen isotope composition versus average SiO_2 contents in the investigated mineral fractions of the 1994 – 1998 calc-silicate xenoliths are plotted in Figure 6, and the new data are reported in Table 2. Various mineral fractions of the xenolith samples are enriched in ^{18}O relative to mantle-derived rocks (5.6 – 6.1 ‰, e.g., Harmon and Gerbe, 1992). The lowest $\delta^{18}O$ values are characteristic of titanomagnetites (6.5 ‰), whereas the highest $\delta^{18}O$ values are typical of the wollastonite-bearing assemblages (8.7 – 17.2 ‰). Notably, virtually all of the calc-silicate mineral fractions give $\delta^{18}O$ values above the range recorded in the recent Javanese volcanic rocks (5.6 – 6.1 ‰, Harmon and Gerbe, 1992; Handley et al., 2010, 2014; Jeffery et al. 2013; Fig. 6). Wollastonite is the most abundant phase in the core part of the MXCS-1 sample (Chadwick et al., 2007). The arrow in the Figure 6 plotted based on the compositions of the analyzed samples indicates consumption of grossular during partial melting that is likely responsible for crystallization of the xenocrystic anorthite (see section 4.3). Assuming that (1) anorthite was in equilibrium with water-rich fluid, (2) pure grossular (Grs) had $\delta^{18}O_{Grs}$ = 10.21‰ (Table 2), and (3) $\Delta_{An\text{-}H2O} = -1.04$ ‰, $\Delta_{Grs\text{-}H2O} = -2.13$ ‰ at 1100°C, and $\Delta_{An\text{-}H2O} = -1.16$, $\Delta_{An\text{-}H2O} = -2.53$ at 900°C (Zheng, 1993), the calculated oxygen isotope composition of anorthite in the calc-silicate xenoliths, $\delta^{18}O_{An,}$ would have to vary from 11.3 to 11.6 ‰.

4.3. Thermodynamic modelling using the Magma Chamber Simulator

Thermodynamic modelling of energy- and mass- constrained assimilation and fractional crystallization (the Magma Chamber Simulator, MCS, Bohrson et al., 2014) has been applied to constrain the origin of the anorthite-rich plagioclase. In the MCS, thermal energy from cooling and crystallization of a magma body heats up and potentially melts wallrock. Most of the associated anatectic melt is mixed with magma body melt. Equilibrium crystal+melt±volatile conditions are calculated for each step of assimilation and fractional crystallization until the magma body-wallrock composite system reaches thermal equilibrium. We used two known compositions (contrasting Ca-rich and Si-rich end-members) of the calc-silicate xenoliths from the 1998 Merapi collection (MXCS-1R; MXCS-4, respectively; Chadwick et al., 2007), the composition of melt inclusions AF11 and Test1-21 of Borisova et al. (2013) (Table A4), as well as the composition of mafic rock reported in the experimental work of Pichavant et al. (2002) to represent a hydrous mafic arc magma (SV1/2 dark scoria, Table A4; Fig. 7). This mafic composition corresponds to Mount Pelée (Martinique, Lesser Antilles Arc) but serves here as an example of a hydrous mafic arc magma that crystallizes high-anorthite plagioclases. We chose this composition as the parent because of the available experimental data and its major element resemblance to the Merapi eruptive products (Fig. A4). These compositions as well as input parameters are presented in the Figure A4 and Table A4 (Electronic Appendix). In the MCS model, the percolation threshold ($f_{\ell,crit}^{WR}$) required for transfer of wallrock melt to the magma body was set to 0.02 (2%) instead of the more typical 0.08 (8%) defined by Bohrson et al. (2014) because of the high mobility of carbonated melts (e.g., Minarik, 1998; Blythe et al., 2015) and to be consistent with the condition required by MCS code: $WR_{Liquid}\% \geq f_{\ell,crit}^{WR}$, where $WR_{Liquid}\%$ is percentage of partial melt produced in the

wallrock (WR). The following initial parameters have been assumed: Fe_2O_3/FeO ratio = 0.24, P_2O_5 = 0.1 wt.% and H_2O = 3 to 4 wt.% (water content was chosen to be close to the water-rich fluid saturation of melt according to the results of Costa et al. (2013) and Borisova et al. (2013)). The models were run at isobaric conditions of 200 MPa. Figure 7 demonstrates that anorthite-rich plagioclases may crystallize from hydrous mafic magma (basaltic andesite melt system, Model M11, Table A4) at temperatures of ~1100°C. Similar anorthite-rich plagioclase is also stable in the assimilated Si-rich and Ca-rich calc-silicate wallrock as grossular is consumed during wallrock partial melting (at ~900°C in the models M5, M7, M11). Moreover, Model M11 with basaltic andesite magma requires ~17 wt.% of the wallrock melt to be added to the 2010 Merapi magma. This result is in agreement with estimates of 15 – 40 wt.% crustal assimilation degree (*F*) obtained by Borisova et al. (2013). Because of rapid heat diffusion (e.g., Edwards and Russell, 1998), the calc-silicate material would rapidly reach temperatures of ~900°C upon magma-wallrock interaction, suggesting effective partial melting and dissolution of the crustal xenoliths. Thus, the MCS results predict two origins for anorthite-rich plagioclase in the Merapi magma: (i) as xenocrysts due to the wallrock partial melting and (ii) magmatic due to hydrous mafic magma crystallization.

5. DISCUSSION

5.1. Origin of anorthite-rich cores

The anorthite-rich cores in the recent (1994 – 2010) Merapi plagioclase crystals have been considered as xenocrysts derived from calc-silicate xenoliths (Chadwick et al., 2007) or newly formed (idiomorphic) crystals related to calc-silicate assimilation (Deegan et al., 2010;

Borisova et al., 2013; Costa et al., 2013). According to Costa et al. (2013) and Borisova et al. (2013), the 2006 – 2010 anorthite cores might have been produced in a pressure range of 200 – 300 MPa, suggesting that crustal assimilation occurred at depth between 6 and 9 km. Therefore, it was initially hypothesized that the anorthite cores may be enriched in ^{18}O due to interaction between the Merapi magma and assemblages from calc-silicate xenoliths. However, as observed in the present high spatial resolution work on the 2010 Merapi plagioclases, low values of $\delta^{18}O$ = 4.6 – 6.6 ‰ are typical for the anorthite-rich cores (An_{82-97}), whereas the higher values of $\delta^{18}O$ up to 7.9 ‰ belong to the anorthite-poorer zones that are typically found in the rim zones (An_{33-86}) of the studied plagioclase (Fig. 8).

Although the low-$\delta^{18}O$ plagioclase crystals (as low as 4.2 ‰) may be interpreted as crystals that originated from serpentinite- or subducted slab-derived melts (Martin et al., 2011; Jacques et al., 2013), five other hypotheses can be proposed for the 2010 Merapi plagioclases. The anorthite-rich cores may thus represent 1) xenocrysts released from typical Merapi calc-silicate xenoliths; 2) peritectic crystals resulting from either partial melting or dissolution of metamorphic grossular-bearing calc-silicate crust due to its interaction with the 2010 Merapi magma; 3) xenocrysts having high-temperature, hydrothermal origin; 4) crystal fragments or antecrysts from a deep progenitor magma directly derived from a subducting slab; and finally 5) crystals of a recharge hydrous mafic magma (e.g., being similar to the proposed allivalite cumulate origin; Plechov et al., 2008). Below, we discuss each possibility in more detail.

5.1.1. Xenocryst origin

A xenocrystic origin for the Merapi anorthite-rich cores in the 1994 and 1998 eruptions, issued from crustal calc-silicate material, was initially discussed by Chadwick et al. (2007)

and later supported by Deegan et al. (2010). Their arguments are based on *in situ* Sr isotope data acquired from the plagioclase phenocrysts of these earlier Merapi eruptions as well as arguments from experiments simulating interaction between the Merapi calc-silicate xenoliths and silicate melt. Two lines of evidence do not support this origin for the 2010 anorthite crystals. (i) The $\delta^{18}O$ values of the silicate fractions from the 1994 – 1998 Merapi xenoliths are high (8.7 – 17.2 ‰, Fig. 6); thus, crustal anorthite $\delta^{18}O$ values must also be high ($\delta^{18}O_{An}^{calc}$ vary from 11.3 to 11.6 ‰). In reality, the anorthite-rich cores of the 2010 Merapi plagioclases are relatively low in $\delta^{18}O$ (4.6 – 6.6 ‰; Figs. 3 – 5, 8) that rules out the possibility of the direct xenocrystic origin. (ii) If the anorthite-rich plagioclases are indeed xenocrysts coming from the calc-silicate xenoliths, they are expected to have been growing in association with grossular and likely with sphene and apatite, as predicted by the MCS modeling (Table A4). However, neither grossular, sphene nor apatite were found as mineral-hosted inclusions in the investigated 2010 Merapi plagioclase phenocrysts, precluding xenocrystic origin of the high-anorthite cores.

5.1.2. Peritectic origin due to interaction between calc-silicate metamorphic crust and Merapi melt

Chadwick et al. (2007) have demonstrated that the 1994 – 1998 Merapi plagioclase have radiogenic Sr isotope compositions ($^{87}Sr/^{86}Sr$ = 0.7058 – 0.7063) and concluded that they could be related to the assimilation of calc-silicate metamorphic material by the magma. The internal patchy texture of the M2010GR-a and M2010PF-b1 crystals studied here (Figs. 3 and 5) can be interpreted to support a peritectic reaction origin (e.g., Erdmann et al., 2012) i.e., as a result of assimilation of partial melt (or dissolution) of calc-silicate crust. Similarly, the presence of melt inclusions in the central zone of the M2010GR-a crystal (Fig. 3, Table 3)

may imply either partial resorption of plagioclase or, alternatively, formation of melt inclusions that could be ascribed to a peritectic reaction between calc-silicate crustal material and 2010 Merapi melt. If crustal melting caused crystallization of anorthite-rich cores, then the process may be described by the following reaction in accordance with the MCS thermodynamic modelling (see below):

$$\left[Ca_3Al_2\left(SiO_4\right)_3\right]^{Grs}_{Crust} = \left[Ca_3Al_2\left(SiO_4\right)_3\right]^{L}_{Crust} = \left[CaAl_2Si_2O_8\right]^{An}_{Crust/Magma} + \left[Ca_2SiO_4\right]^{L'}_{Crust/Magma} \quad (9),$$

where $\left[Ca_3Al_2\left(SiO_4\right)_3\right]^{Grs}_{Crust}$ is grossular component of the calc-silicate crustal garnet, $\left[Ca_3Al_2\left(SiO_4\right)_3\right]^{L}_{Crust}$ is a pure grossular melt generated by the garnet dissolution in the crustal wallrock material, $\left[CaAl_2Si_2O_8\right]^{An}_{Crust/Magma}$ is anorthite molecule forming plagioclase in either crust or magma-crust contact zone, and $\left[Ca_2SiO_4\right]^{L'}_{Crust/Magma}$ represents the Ca-rich component remaining in the reaction melt (L') in either the crust or the contact zone. Because the Ca-rich melt (L') is in equilibrium with anorthite and is mixed with the magma, anorthite can crystallize at the magma-crust contact zones. Another important issue predicted by the MCS modelling is that the anorthite-rich plagioclase (≥90 mol.% An) must continue to crystallize in the wallrock even after complete consumption of the crustal grossular-rich (Grs_{97}) garnet (Fig. 7), likely due to the liberation of Ca-rich melts (L and L' in the Eqn. 9) with SiO_2 = 54 – 74 wt.%, CaO = 5.9 – 24 wt.% and CaO/Al_2O_3 = 0.4 – 9 that were percolating into the magma from the carbonate-rich wallrocks.

According to the experimental data on equilibrium partitioning of CaO and Na_2O between calcic plagioclase (An_{90-95}) and hydrous silicate glass (with 5 – 7 wt.% H_2O) (Martel et al., 2006), the calculated CaO/Na_2O (wt. %) ratios in the equilibrium melts can vary from 4

to 11 (Table 4). The CaO/Na_2O (2 – 8) ratios of previously described natural augite-hosted calcic melt inclusions and matrix glasses (SiO_2 contents of 61 – 64 wt.%, CaO contents of 5.5 – 10.5 wt.%, Borisova et al., 2013) agree well with the experimental range noted above, thereby suggesting that the natural calcic melts may have crystallized anorthite-rich plagioclases. However, this suggestion is not consistent with the new data on melt inclusions found in the anorthite-rich parts of plagioclase M2010GR-a ($An_{82–92}$, Table 3). While the new melt inclusions have similar SiO_2 (58 – 65 wt.%) to experimental ones, their lower CaO = 1.8 – 5.7 wt.% and CaO/Al_2O_3 = 0.1 – 0.3 are at variance with those of the theoretical Ca-rich grossular-derived melts (CaO of 5.9 – 24 wt.% and CaO/Al_2O_3 of 0.4 – 9) and natural calcic glass inclusions in augite (CaO = 5.5 – 10.5 wt.% and CaO/Al_2O_3 = 0.5 – 1.2; Borisova et al., 2013). Thus, our new data on the glass inclusions hosted by anorthite-rich plagioclase ($An_{82–92}$, Table 3) suggest that the anorthite-rich cores may not be ultimately peritectic crystals originated during partial melting of the upper crustal calc-silicate wallrocks. Moreover, the new oxygen isotope data on the anorthite-rich cores depleted in ^{18}O (Fig. 8) do not favor this hypothesis.

5.1.3. High-temperature, hydrous origin at crustal and mantle depths

Although low-$\delta^{18}O$ values (down to 4 ‰) are known in some Javanese high-temperature crustal rocks (i.e., cordierite- and tridymite-bearing xenoliths; Gardner et al., 2013), no data exist on the assimilation of such high-temperature crust by the Merapi magmas (e.g., Troll et al., 2013). Python et al. (2007) have demonstrated that mantle diopsidites are produced where anorthite coexists with diopside due to high-temperature fluid circulation at mantle conditions in a spreading-related geodynamic setting. However, such mantle anorthites ($An_{93–100}$) are depleted in FeO (<0.09 wt.%) relative to anorthite-rich plagioclase found in the 2010 Merapi

eruption. In this work, we infer that the moderate to high FeO (0.2 – 0.8 wt.%) contents and low to moderate $\delta^{18}O$ (4.6 to 6.6 ‰) values in the anorthite-rich cores (An_{82-97}) (Figs. 3 – 5) can be explained by interaction of mantle-derived magma (5.6 – 6.1 ‰, e.g., Harmon and Gerbe, 1992) with an old high-temperature lithology depleted in ^{18}O (e.g., Harris and Ashwal, 2002; Suzuki et al., 2015). Thus, the 2010 Merapi anorthite-rich cores were likely crystallized at hydrous conditions (in particular, up to melt saturation with water-rich fluid) because high water activity at high-temperature conditions is favorable for crystallization of anorthite-rich plagioclases in different geodynamic settings (e.g., Bindeman and Bailey, 1999; Feig et al., 2006; Plechov et al., 2008).

5.1.4. Closed-system crystallization of the 2010 Merapi basaltic andesite

It is well known that world-wide, serpentinites, eclogites and slab-derived melts may be strongly depleted in ^{18}O and have $\delta^{18}O$ values (down to ~3 – 4 ‰) remarkably lower than that of typical mantle (e.g., Bindeman et al., 2005, Bindeman, 2008; Martin et al., 2011; Jacques et al., 2013). Thus, the values of $\delta^{18}O$ down to 4.6 ‰, which are signatures of the 2010 Merapi anorthite cores ($An_{82–97}$), may be potentially attributed to slab-derived melts. Possible candidates are adakite-type magmas considered as slab-derived magmas. However, several lines of evidence allow us to rule out this possibility. First, plagioclase crystallizing from adakite-type magmas usually has lower anorthite contents (An_{27-80}) (e.g., Prouteau and Scaillet, 2003; Jamshidi et al., 2015) than the 2010 Merapi plagioclase cores. Second, it seems to be problematic to produce the anorthite-rich plagioclases ($An_{\geq 90}$) by closed-system crystallization of the bulk-rock 2010 Merapi basaltic andesite at any crustal depths, as shown by Costa et al. (2013). Third, the character of the 2010 plagioclase zoning points towards magma recharge and resorption processes that may occur in the Merapi plumbing system (see

Figs. 3 and 5). We, thus, suggest open-system crystallization of anorthite-rich cores rather than closed-system crystallization directly from the 2010 Merapi basaltic andesite melt.

5.1.5. Open-system crystallization of the 2010 Merapi basaltic andesite

Plagioclase with anorthite-rich composition crystallizing from a hydrous mafic magma is expected to have mantle-like $\delta^{18}O$ values and high FeO contents (Borisova et al., 2013), that are due to magma derivation or equilibration with Javanese upper mantle (5.6 – 6.1 ‰, e.g., Harmon and Gerbe, 1992). If so, such plagioclases produced in a deep magma chamber (~400 MPa and ~1000 °C; Pichavant et al., 2002) or at shallower level (~200 MPa and ~900 °C; Martel et al., 2006) from hydrous basalt or basaltic andesite melt, would have also high FeO contents. The moderate to high FeO (0.2 – 0.8 wt.%) contents in the three 2010 Merapi anorthite-rich cores (An_{82-97}) overlap those of calcic plagioclases (An_{84-95}, 0.8 – 0.9 wt.% FeO) from the experiments of Pichavant et al. (2002) that ran at hydrous conditions ($\alpha_{H2O} \leq 1$). Moreover, the concentrations of FeO in the Merapi anorthite-rich plagioclases are in the range that is typical for calcic plagioclase cores of the Mt. Pelée lavas (Pichavant et al., 2002). Our calculations of FeO contents in the Merapi mafic melt using experimental coefficients of Bindeman et al. (1998) and data of Pichavant et al. (2002) on Fe partitioning (0.08 – 0.11) between calcic plagioclases (An_{82-97}) and mafic melts, either dry or hydrous, suggest that the Merapi melt must have had 1.4 – 10 wt.% FeO contents (Table 4). New melt inclusions analyzed in the anorthite-rich ($An_{82–92}$) zone of the M2010GR-a plagioclase are characterized by variable FeO (2.1 – 6.4 wt.%) contents (Table 3), which match the proposed signature of the anticipated mafic melt. The entrapped melts have trachyandesite composition, with 58 – 65 wt.% SiO_2 contents, that may be more evolved compared to the initially entrapped melt due to post-entrapment crystallization of plagioclase inside the inclusion hosted by anorthite-rich crystal. Thus, the FeO contents measured in three plagioclase crystals and the anorthite-rich-hosted melt inclusions support the validity of the mafic magmatic hypothesis, suggesting recharge of hydrous melts having likely basalt through basaltic trachyandesite composition.

Thus, the following equation describing crystallization of An-rich plagioclase may be suggested:

$$\left[CaAl_2Si_2O_8\right]^{L}_{RechargeMagma} = \left[CaAl_2Si_2O_8\right]^{An}_{RechargeMagma} \quad (10),$$

where $\left[CaAl_2Si_2O_8\right]^{L}_{RechargeMagma}$ represents the anorthite component of the initial L melt of the recharge mafic magma and $\left[CaAl_2Si_2O_8\right]^{An}_{RechargeMagma}$ is the anorthite component of the plagioclase crystal produced during the reaction. It should be noticed here that in the Kuriles, Kamchatka, Lesser Antilles, and Japan there are "allivalites" containing abundant An-rich plagioclase and forsterite-rich olivine (e.g., Bindeman and Bailey, 1999; Plechov et al., 2008) that belong to cumulative troctolite assemblage. These anorthitic plagioclases have been interpreted as produced from hydrous (e.g., mafic) magma. Thus, the Merapi anorthite-rich cores may have similar origin due to open-system crystallization from a recharge mafic melt.

It is also worth emphasizing that MCS thermodynamic modelling performed at 200 MPa is generally consistent with the hydrous mafic hypothesis (Fig. 7). Based on the experimental data of Pichavant et al. (2002), we predict that hydrous mafic melts would crystallize anorthite-rich plagioclase ($An_{>90}$) at pressures greater than 200 MPa. Our hypothesis is in agreement with the available data of Chadwick et al. (2013) on Merapi anorthite-bearing gabbroic and anorthosite igneous inclusions. According to Chadwick et al. (2013), these igneous (felsic and mafic plutonic) inclusions, where anorthite is an abundant mineral phase, could have crystallized at ~200 – 600 MPa in the Merapi plumbing system (Fig. 9). Thus, we ascribe the formation of the Merapi anorthite cores to open-system crystallization from a hydrous basaltic or basaltic trachyandesite melt that recharged the 200 – 600 MPa magma reservoir rather than from the upper calc-silicate crust involved into the 2010 Merapi pre-eruptive magma at 925 – 950°C and 100 – 200 MPa (Erdmann et al., 2016).

5.2. Role of crustal assimilation in oxygen isotope heterogeneity of the 2010 Merapi magma

The previously analyzed bulk 2010 samples comprising ash, pyroclastic flow and tephra materials yielded $\delta^{18}O$ values of 5.6 to 6.9 ‰ (Borisova et al., 2013; Troll et al., 2013). This indicates a slight shift to lower $\delta^{18}O$ values relative to those previously reported for Merapi volcanic products (6.0 to 8.3 ± 0.1 ‰). Moreover, the average $\delta^{18}O$ was measured consistently at 6.5 ± 0.1 ‰ in two monomineralic fractions of the 2010 plagioclase, suggesting that the equilibrium melt must have $\delta^{18}O$ of 6.9 ± 0.3 ‰, given the uncertainties associated with the average melt composition, the bulk plagioclase (anorthite content), and estimates of equilibrium temperature (Zhao and Zheng, 2003). In contrast to the Javanese rock and crystal data (e.g., Troll et al., 2013), the silicate fractions of the 1994 – 2006 Merapi calc-silicate xenoliths display more positive $\delta^{18}O$ values (Fig. 6), suggesting the calc-silicate assemblage-derived melt to be enriched in ^{18}O isotope. Indeed, a wide range of $\delta^{18}O$ values, from 6.5 ‰ to 17.2 ‰, was recorded in the 1994 – 1998 Merapi calc-silicate-derived titanomagnetite-bearing and wollastonite-bearing mineral fractions (Fig. 6, Table 2). The strong contrast between oxygen isotope compositions of the Merapi magmatic products and the crustal calc-silicate xenoliths is expected to generate significant $\delta^{18}O$ heterogeneity in the pre-eruptive magma at crustal levels. The most probable mechanism of contamination of the 2010 Merapi magma is mixing of crust-derived calcic melt (representing crustal assimilant) with a juvenile, K-Cl-rich, hydrous silicic melt at pre-eruptive conditions (Borisova et al., 2013). If so, the $\delta^{18}O_{melt}$ can be calculated using plagioclase (anorthite, An) – melt (andesite) fractionation factor ($\Delta^{18}O_{An\text{-}melt} \approx 1000\ln\alpha_{An\text{-}melt}$ = -0.3‰ at 950°C, where $\alpha_{An\text{-}melt}$ =

$(^{18}O/^{16}O)_{An}/(^{18}O/^{16}O)_{melt}$; Zhao and Zheng (2003)). The following two-component mixing model (Eqn. 11) for oxygen isotopes (Borisova et al., 2013) allows us to estimate the degree of the 2010 Merapi magma contamination with the calc-silicate material.

$$F = \left(C^{Init}_{melt}R^{Init}_{melt} - C^{Init}_{melt}R^{Hybr}_{melt}\right) / \left(C^{AssimAll}_{melt}R^{Hybr}_{melt} - C^{Init}_{melt}R^{Init}_{melt} - C^{AssimAll}_{melt}R^{Assim}_{melt} + C^{Init}_{melt}R^{Init}_{melt}\right) \quad (11),$$

where F is the fraction of crustal assimilant integrated into the hybrid magma (represented by hybrid melt mixed with hybrid phenocrysts and ranging from 0 to 1); C^{Init}_{melt} is the average concentration of an element in the initial melt; R^{Init}_{melt} is the initial isotopic ratio in the melt before assimilation; R^{Hybr}_{melt} is the isotopic ratio in hybrid melt; R^{Assim}_{melt} is the isotopic ratio in crustal assimilant melt; and $C^{AssimAll}_{melt}$ is the average concentration of an element in the crustal assimilant melt. Assuming R^{Init}_{melt} (Fig. 6) varies from 4.9 to 5.6 ‰ for $\delta^{18}O$ (i.e., the lowest "mantle-like" $\delta^{18}O$ = 4.6 – 5.3‰ values belonging to An-rich zones of the 2010 plagioclase crystals), R^{Hybr}_{melt} (for mixed or hybrid melt) for $\delta^{18}O$ varies from 5.6 to 6.9‰ (the 2010 bulk rock values according to Borisova et al., 2013; Troll et al., 2013), R^{Assim}_{melt} (for assimilant melt) ranges from 12.1 to 18.3‰ (calculated according to 11.0 to 17.2‰ $\delta^{18}O$ in the clinopyroxene-bearing mineral fractions of the calc-silicate xenoliths, $\Delta^{18}O_{Di\text{-}melt} \approx 1000\ln\alpha_{Di\text{-}melt}$ = -0.8‰ at 950°C, Zhao and Zheng (2003)), $C^{AssimAll}_{melt}$ (for the bulk assimilant melt) is 41 – 46 (wt. %), and C^{Init}_{melt} is 40 – 45 (wt. %), in the Eqn. 11, the final F ranges from 0.02 to 0.30.

These simple calculations suggest that the pre-eruptive Merapi magma might have assimilated up to 30 wt.% of calc-silicate crustal material. MCS modelling with basaltic andesite magma requires 17 – 18 wt.% of the wallrock liquid added to the 2010 Merapi magma (Table A4). Our data are in a good agreement with the previous conclusion of Borisova et al. (2013) (based on Sr isotopic and Sr elemental concentration data) that 15 to 40 wt.% of crustal calc-silicate material was assimilated by pre-eruptive basaltic andesite magma

prior to the 2010 Merapi eruption. We thus conclude that assimilation of ~18 wt.% of the calc-silicate crustal material would be consistent with oxygen isotope heterogeneity of the melt recorded in plagioclase phenocrysts.

5.3. General model of open-system crystallization

Figure 9 is a schematic illustration outlining our preferred model. It is based on our evidence that crystallization of the 2010 Merapi high-anorthite plagioclase occurred from recharge of hydrous mafic melts into the Merapi magma reservoir system. This evidence is independently supported by Sr isotope data of Merapi plagioclases and bulk-rock products. The anorthite-rich plagioclase is present in the core parts of the crystals, whereas the sodic plagioclase is associated with the rim parts. Therefore, we infer that the anorthite is an early-stage magmatic plagioclase crystallized from recharge, of hydrous basaltic to basaltic trachyandesite melt; in contrast, the late-stage sodic plagioclase originated from silicic melts affected by upper crustal calc-silicate assimilation (see calcic melt inclusions in Table 4 of Borisova et al., 2013). The early-stage anorthite-rich cores crystallized at 200 – 600 MPa, likely corresponding to the main reservoir where plagioclase growth dominated (Chadwick et al., 2013). The late-stage sodic plagioclases have crystallized at shallow crustal level (100 – 200 MPa), corresponding to the 2010 Merapi pre-eruptive conditions in the upper carbonate crust. The compositional contrast between the high-anorthite cores growing deeper in the crust and sodic plagioclase rims crystallizing within shallower carbonate crust is likely related to the bulk H_2O versus CO_2 contents in the Merapi magmatic system. High H_2O content is favorable for anorthite crystallization (at deeper levels; Sisson and Grove, 1993), whereas increased CO_2 (low H_2O)

partial pressure related to carbonate assimilation would trigger more sodic plagioclase crystallization at shallower crustal levels.

Slightly radiogenic $^{87}Sr/^{86}Sr$ (0.7057–0.7060) in the bulk-rock 2010 Merapi products has been considered as reflecting irrefutable evidence for the carbonate crust assimilation (Borisova et al., 2013). According to Chadwick et al. (2007), the 1994-1998 Merapi high-anorthite cores are slightly more radiogenic $^{87}Sr/^{86}Sr$ (0.7058 – 0.7068) than plagioclase rims (0.7057 – 0.7060). The bulk-rock Sr isotope ratios (0.7050 – 0.7058) of the historic Merapi volcanics analyzed by Gertisser and Keller (2003) and Debaille et al. (2006) are even lower than those of the 1994-1998 Merapi plagioclase rims, suggesting participation of at least two different sources for the bulk-rock Sr isotope signatures or variables amounts of assimilation into the Merapi magmas. In this context, the elevated $^{87}Sr/^{86}Sr$ ratios in the recent Merapi bulk-rock volcanic products reflect two origins of the plagioclases: (1) as xenocrysts, sourced from a sedimentary protolith, that have high $^{87}Sr/^{86}Sr$, high An mol.% content (Chadwick et al. 2007); or (2) due to crustal assimilation with combined fractional crystallization forming magmatic rims and reaction zones with increasing $^{87}Sr/^{86}Sr$ and decreasing An mol.% content in the rims (see Fig. 6a in Chadwick et al., 2007). Our study based on *in situ* $\delta^{18}O$ measured in the plagioclase phenocrysts supports the second scenario for the 2010 Merapi high-anorthite cores. During early crystallization at deeper crustal level of 200 – 600 MPa, plagioclase chemical signatures are dominated by growth in hydrous mafic magmas that evolve as crystallization continues (Fig. 9). Low to moderate $\delta^{18}O$ (4.6 to 6.6 ‰) values in the anorthite-rich cores (An_{82-97}) are explained by interaction of mantle-derived magma with an old high-temperature lithology depleted in ^{18}O (see section 5.1.3; Harris and Ashwal, 2002; Suzuki et al., 2015). Magmas then ascend to shallower levels (100 – 200 MPa), undergoing continued plagioclase growth and interaction with the calc-silicate crust that yield higher $^{87}Sr/^{86}Sr$ and $\delta^{18}O$ in the crystal rims and reaction zones (An_{33-86}).

5.4. Timescale of magma recharge and crustal assimilation

Available data on the growth rate of plagioclases (e.g., Kirkpatrick, 1981; Cashman, 1993), which can be used to constrain the timescale of the anorthite-rich core formation demonstrate that the rates of plagioclase growth vary from ~10^{-9} to ~10^{-5} mm/s, and are a function of temperature, melt composition, partial H_2O pressure and degree of supercooling (ΔT) (Kirkpatrick, 1981). Moreover, the experimental data of Sato et al. (1981), Lofgren (1980) and Mollard et al. (2012) have shown that plagioclase growth rate is reflected by the crystal habits, being ~5×10^{-7} to 1×10^{-6} mm/s at $\Delta T = 40°C$ supercooling for tabular plagioclase crystals that form from hydrous silicate melts. Applying these data to the investigated 2010 Merapi plagioclase of tabular habit with average size of 1300 µm (i.e., and suggesting constant rate of 5×10^{-7} to 1×10^{-6} mm/s), the Merapi anorthite-rich cores of 1 mm size might have formed over 15 – 30 days. This is a minimum estimate because the real rate of crystallization was not constant (slowing down with decrease in ΔT and resorption events). For example, assuming plagioclase growth rates of 10^{-7} to 10^{-9} mm/s (Cooper & Kent, 2014) results in growth durations of months (0.4 yr) to years (32 yr).

Given similarities between the ^{18}O and Fe diffusion coefficients in calcic plagioclases (Cherniak, 2010; Farver, 2010), the documented strong variations in $\delta^{18}O$ (from 4.6 to 7.9 ‰) and poor FeO_{Plag} variations (in the limit of analytical uncertainty) suggest that oxygen isotope heterogeneity and unsystematic FeO_{melt} variations (limited between 1.4 and 10 wt.% FeO contents, see section 5.1.5) persisted during plagioclase growth. Indeed, the analyzed plagioclase-hosted melt inclusions show variable FeO_{melt} from 2.1 to 6.4 wt.% contents (Table

3; Borisova et al., 2013). We can use the scale (width, size) of the oxygen isotope heterogeneity as a proxy to estimate survival timescale with respect to $\delta^{18}O$. We used the unique available dataset on oxygen isotope diffusion in anorthite crystals in direction parallel to *c* axis of Elphick et al. (1988) at high temperatures overlapping the 2010 Merapi magma temperature range and the equation (2.15) of Crank (1975) suggesting x = h, transforming the equation to:

$$C / C_o = 0.5 \{\mathrm{erf}\,(2h) \;/\; (2\sqrt{Dt})\}, \quad (12),$$

where *t* (s) is time of complete homogenization by chemical diffusion, 2h (m) is peak length derived from 2h = 50 μm scale (see Figs. 3 – 5; Table 5), and *D* (m^2/s) is calculated as:

$$D = D^{\circ} e^{(-Q / (RT))} \quad (13),$$

where D° (m^2/s) is nominal diffusion rate, Q (kJ/mol) is activation energy, T is temperature (K) and R (8.31E-03 kJ/molK) is ideal gas constant. Using the available data of Elphick et al. (1988) on ^{18}O diffusion in anorthite at high temperatures and equations 12 and 13, the timescale of the oxygen isotope heterogeneity at 50 μm scale is 34 yrs (at maximal temperature of 1100°C) (Table 5).

The estimated timescale of the documented $\delta^{18}O$ heterogeneity corresponds to the timescale of the 2010 plagioclase growth and residence, starting from its crystallization due to mafic magma recharge at higher pressures (200 – 600 MPa) in a magma reservoir(s) (Fig. 9) until calc-silicate crustal assimilation (100 – 200 MPa) and rapid cooling of the host magma due to explosive eruption. Thus, this calculated timescale for oxygen isotope heterogeneity (Figs. 3 – 5) is thought to reflect the crystallization and eruption time spans of the plagioclase,

starting from the crystal core formation till the eruption. If the recharge basaltic andesite magma temperature of 1100 °C at ≥200 MPa is assumed (Fig. 7), the magma recharge and crustal assimilation appeared to be a relatively rapid process acting on a timescale shorter than 34 yrs. We note that these timescales are in accordance with the estimates of the 2010 Merapi clinopyroxene residence timescales (1.6 – 2.7 years; Costa et al., 2013) at conditions preceding the eruption. The estimated timescales shorter than 34 yrs are also in accord with crystal size distribution data of van der Zwan et al. (2013) that yields timescales of 5 to 31 yrs for the Merapi plagioclase crystallization induced by the ascent and degassing.

6. SUMMARY AND CONCLUSIONS

1) The present *in situ* microanalytical study revealed stronger variations of oxygen isotopes ($\delta^{18}O_{SMOW}$) in the 2010 Merapi plagioclases at a micrometer-scale as compared to the grain-scale (analyzed by laser fluorination). The oxygen isotope variations suggest contributions of three principal sources of oxygen ions into the Merapi plumbing system, implying at least two principal sources of volatile oxides (especially, CO_2): crust and mantle.

2) The discovered strong $\delta^{18}O$ variability in the 2010 Merapi plagioclases suggests oxygen isotope heterogeneity of the magma that persisted during most of plagioclase growth time at depth. Open-system processes, i.e., magma recharge and crustal assimilation coupled with fractional crystallization, were likely responsible for the oxygen isotope variations from 4.6 to 7.9 ‰ $\delta^{18}O$ in the plagioclase crystals grown at 925 – 1100°C and 100 to 600 MPa in the magma chamber(s) associated with the 2010 Merapi eruption.

3) Magma Chamber Simulator thermodynamic modelling is consistent with assimilation of ~18 wt.% of crustal calc-silicate material by the 2010 Merapi basaltic andesite magma preceding eruption. The lowest values of $\delta^{18}O$ (4.6 – 6.6 ‰) are typical for the anorthite-rich cores ($An_{82–97}$), whereas the higher values of $\delta^{18}O$ (5.7 – 7.9 ‰) were found in the anorthite-poorer (frequently rim) zones ($An_{33–86}$) in all three analyzed plagioclases. Our data do not support that the anorthite-rich cores ($An_{82–97}$) formed as xenocrysts due to partial melting and associated disaggregation of upper crustal carbonate material. The anorthite-rich cores ($An_{82–97}$) originated as abundant early-stage calcic plagioclase crystallized from hydrous recharge mafic (basaltic or basaltic trachyandesite) melt, which might be affected by assimilation of an old lower crustal high-temperature lithology (at ~ 1100°C, 200 – 600 MPa). In contrast, the late-stage sodic plagioclase ($An_{33–86}$) rims were likely crystallized from more silicic melt affected by calc-silicate crustal assimilation at shallow crustal levels (at 925 – 950°C, 100 – 200 MPa).

4) Our estimations of survival timescale of ^{18}O heterogeneity in the anorthite-rich cores based on available ^{18}O diffusion data in anorthite imply that the entire time span for plagioclase crystallization (and related recharging and crustal assimilation preceding the 2010 Merapi eruption) and residence till magma eruption were limited to 34 yrs.

5) Magma Chamber Simulator modeling infers two possible origins of plagioclases in Merapi plumbing system: (1) as predominant phenocrysts due to hydrous mafic magma recharge and crystallization at 200 – 600 MPa (investigated in this work); and (2) as minor xenocrysts due to partial melting/dissolution of the calc-silicate wallrocks at 100 – 200 MPa (found and investigated by Chadwick et al., 2007).

ACKNOWLEDGEMENTS

The authors thank the journal editors, Marc Norman and Janne Blichert-Toft as well as F.J. Tepley, T. Waight and one anonymous reviewer for editorial comments and suggestions on the earlier versions of this paper. AYB thanks I. Bindeman, E. Deloule, P. de Parseval, J. Schott, and V.R. Troll for providing plagioclase reference materials and the Merapi calc-silicate xenoliths for this work and F.M. Deegan for preparation of the calc-silicate xenolith samples. I. Bindeman, S. Erdmann, G. Pokrovski, J. Schott and V.R. Troll are thanked by AYB for continuous discussion on the earlier versions of the manuscript. C. Cavare-Hester is thanked for help in figure drawing. Authors thank the financial support of the Institut National des Sciences de l'Univers (INSU, France), project “AO ALEAS” (2014), “AO CESSUR” (2015) and financial support from Université Federale de Toulouse (2015) to A.Y.B., and ANR project “DOMERAPI” (2012 – 2016) to J.-P. Métaxian. This is the CRPG contribution № 2447.

FIGURE CAPTIONS

Figure 1. (a) Overview map of the Sunda arc, Indonesia. Open circles represent active volcanoes. Merapi volcano in Central Java is indicated by triangle. (b) Simplified locality map of Merapi and surroundings with the location of the investigated samples shown by the open circle. A nearby major population center is the city of Yogyakarta located at 25–30 km to the south. The maps (a and b) are modified after Troll et al. (2013). (c) Photo of Merapi volcano taken from the Gendol River by the first author in September 2015.

Figure 2. Electron microscope (back-scattered electron, BSE) images of (a) M2010GR and (b) M2010PF samples from the 2010 Merapi products. Abundant plagioclase crystals, anorthite-rich cores and complex zoning in the plagioclases are visible in the both images. "Plag" corresponds to the plagioclase phenocrysts and "Cpx" means clinopyroxene crystals.

Figure 3. Zonation of the M2010GR-a plagioclase crystal: (a) Optical microscope transmitted-light and (b) electron microscope (back-scattered electron, BSE) images, with similar scales (×150 magnification); (c) Anorthite (An, in mol.%) and FeO in wt.% zonations along AB profile, and (d) Zonation in $\delta^{18}O$ (in per mil, ‰) along the AB profile. The indicated 1σ error of the $\delta^{18}O$ values is 0.22‰ and 10 μm error bars are for the spatial resolution. A central (An_{51-83}) zone is relatively depleted in anorthite and enveloped by anorthite-rich core (An_{89-93}). See text for discussion. Dashed lines delimit the "2h" scale of isotopic heterogeneity of 50 microns (see section 5.4).

Figure 4. Zonation of the M2010PF-a plagioclase crystal: (a) Optical microscope transmitted-light and (b) electron microscope BSE images, with similar scales (×120 magnification); (c) Anorthite (An, in mol.%) and FeO in wt.% zonations, and (d) Random variations in respect to $\delta^{18}O$ (in per mil,‰) along the AB profile. The indicated 1σ error of the $\delta^{18}O$ values is 0.16‰ and 10 μm error bars are for the spatial resolution. Dashed lines delimit the "2h" scale of isotopic heterogeneity of 50 microns (see section 5.4).

Figure 5. Zonation of the M2010PF-b1 plagioclase crystal: (a) Optical microscope transmitted-light and (b) electron microscope BSE images, with similar scales (×100 magnification); (c) Anorthite (An, in mol.%) and FeO in wt.% zonations, and (d) Random variations in respect to $\delta^{18}O$ (in per mil,‰) along the AB profile. The indicated 1σ error of the $\delta^{18}O$ values is 0.11‰ and 10 μm error bars are for the spatial resolution. The ~170 μm-size central (An_{44-80}) zone relatively depleted in anorthite and enveloped with 400 μm-size anorthite-rich core (An_{88-93}) is likely the signature of the open magmatic system. Dashed lines delimit the "2h" scale of isotopic heterogeneity of 50 microns (see section 5.4).

Figure 6. $\delta^{18}O_{SMOW}$ (in per mil, ‰) versus average SiO_2 contents (wt.%) of the mineral fractions of the 1994 – 1998 Merapi calc-silicate xenoliths. The following abbreviations have been used: "TiMgt" = titanomagnetite; "Grs" = grossular; "Woll" = wollastonite; "Calc" = calcite; "An" = anorthite; "Glass" = silicate glass; "major" means predominant phase. The arrow indicates shift of the bulk grossular-bearing mineral assemblage composition upon interaction of the calc-silicate xenoliths with the surrounding melt. Analysis errors are smaller than the symbol size. Points marked by "(calc)" are the calculated oxygen isotope compositions; see text for details. Dashed lines delimit the silicate-bearing mineral fractions

analyzed by laser fluorination. Fields for Javanese igneous rocks and mantle are after Handley et al. (2010, 2014), Jeffery et al. (2013) and Harmon and Gerbe (1992).

Figure 7. Temperature (T, °C) versus anorthite (An, moles) and grossular (Grs, moles) contents in the crystallizing plagioclases and garnets plotted according to the results of Magma Chamber Simulator modelling performed at 200 MPa pressure. For "plagioclase, hydrous mafic magma crystallization", the major element composition of basaltic andesite (model M11) was used as the initial magma component. Two contrasting calc-silicate xenolith wallrocks (WR) have been used: Si-rich (model M11) and Ca-rich (model M7) end-members (see Table A4 for details). The MCS results predict two origins for anorthite-rich plagioclase in the Merapi magma: (i) as xenocryst due to the wallrock partial melting, and (ii) as phenocrysts due to hydrous mafic magma crystallization. The most critical MCS input parameters and representative results are summarized in Table A4.

Figure 8. $\delta^{18}O_{SMOW}$ (in per mil, ‰) versus anorthite contents (An, in mol.%) in three plagioclase crystal profiles: (a) M2010GR-a AB; (b) M2010PF-a AB; (c) M2010PF-b1 AB. The linear trends plotted between $\delta^{18}O$ and corresponding minimal (and maximal) anorthite contents (An min and An max, respectively) show tendency of negative correlations.

Figure 9. Schematic illustration of the Merapi (Central Java, Indonesia) plumbing system and oxygen isotope signatures of the crystallizing plagioclases. Deeper (200 – 600 MPa, 13 – 20 km) zone corresponds to open-system crystallization of abundant anorthite-rich core from recharge hydrous mafic melt. The deep crustal zone representing the main andesite storage

interval is after Chadwick et al. (2013). Low to moderate $\delta^{18}O$ (4.6 to 6.6 ‰) values in the 2010 Merapi anorthite-rich cores (An_{82-97}) are explained by interaction of mantle-derived magma with lower crustal lithology depleted in ^{18}O due to high temperature alteration. Magmas then ascend to shallower levels (100 – 200 MPa, ~4.5 to 9 km), undergoing continued plagioclase growth and interaction to the calc-silicate crust that yield higher $\delta^{18}O$ (5.7 to 7.9 ‰) in 2010 Merapi anorthite-poorer rims (An_{33-86}). The shallow zone of the middle to upper crust corresponds to the area where crystallization of the 2010 pre-eruptive magma occurs (Erdmann et al., 2016). The illustration is developed after Chadwick et al. (2013).

Figure A1. One-inch polished section sample developed for the current work. The sample consists of: i) central part (10 mm) hosting plagioclase crystals and standards in an epoxy matrix; ii) a peripheral part of Cu-Zn brass, allowing perfect polishing of the whole surface, thus minimizing relief effect necessary for high-resolution analysis (see section 3.5).

Figure A2. Average instrumental mass fractionation (IMF, $\Delta^{18}O_{IMF(RM)}$, in ‰) plotted versus anorthite contents (in mol.%) in four reference plagioclases for three analytical subsets performed in the first analytical session (26 – 29/01/2015). Each calibration was used for each of three natural plagioclase samples profiles (corresponding to the plagioclase sample numbers).

Figure A3. Average instrumental mass fractionation (IMF, $\Delta^{18}O_{IMF(RM)}$, in ‰) for the second analytical session (performed 08 – 09/05/2015) plotted versus anorthite contents (in mol.%) in five reference plagioclases. Two regression lines were plotted: 1) for the four standards (Std

1, 2, 3, 5: blue diamonds) which were used for determinations of the IMF versus anorthite content relationship during the first analytical session; 2) for the five standards (Std 1, 2, 3, 5, 6: red squares). The modelled $\delta^{18}O$ value for the anorthite standard (Std 6) was calculated using its known anorthite content and the eqn. 8, which allowed calculation of the mismatch in $\delta^{18}O$ to that known from laser fluorination analysis (see section 3.6).

Figure A4. Al_2O_3, MgO, CaO, K_2O contents versus SiO_2 contents into the input components used for the MCS modelling in comparison to the composition of the Merapi igneous products. The corresponding compositions are given in Table A4. The chemical data on the Merapi volcanic products were obtained from Borisova et al. (2011; 2013).

Table 1. Instrumental mass fractionation (IMF, $\Delta^{18}O_{IMF}$) for oxygen isotopes in the first analytical session.

Table 2. Oxygen isotope data on the 1994 – 1998 Merapi calc-silicate xenoliths.

Table 3. Composition of glass inclusions in M2010GR-a plagioclase.

Table 4. Partitioning coefficients between plagioclase and melts and the calculated composition of the 2010 Merapi melts.

Table 5. Calculation of timescales based on ^{18}O diffusion in anorthite.

Table A1. Merapi calc-silicate xenolith location and sampling.

Table A2(1-3). Anorthite contents with corresponding $\delta^{18}O_{SMOW}$ isotope data on the 2010 Merapi plagioclases.

Table A3. Instrumental mass fractionation (IMF, $\Delta^{18}O_{IMF}$) for oxygen isotopes in the second analytical session dedicated to estimate accuracy.

Table A4(a). Composition of input components used for the MCS modeling.

Table A4(b). Initial conditions for the most representative Magma Chamber Simulator modelling.

Table A4(c). The most representative results of Magma Chamber Simulator modelling.

REFERENCES

Baertschi P. (1976) Absolute ^{18}O content of Standard Mean Ocean Water, *Earth Planet. Sci. Lett.* **31**, 341–344.

Bindeman I.N., Davis A.M. and Drake M.J. (1998) Ion microprobe study of plagioclase-basalt partition experiments at natural concentration level of trace elements. *Geochim. Cosmochim. Acta* **62**, 1175–1193.

Bindeman I.N. and Bailey J.C. (1999) Trace elements in anorthite megacrysts from the Kurile Island Arc: a window to across-arc geochemical variations in magma compositions *Earth Planet. Sci. Lett.* **169**, 209–226.

Bindeman I. N., Eiler J.M., Yogodzinski G.M., Tatsumi Y., Stern C.R., Grove T.L., Portnyagin M., Hoernle K., Danyushevsky L.V. (2005) Oxygen isotope evidence for slab melting in modern and ancient subduction zones *Earth Planet. Sci. Lett.* **235**, 480–496.

Bindeman I. N. (2008) Oxygen isotopes in mantle and crustal magmas as revealed by single crystal analysis. In: *Minerals, Inclusions and Volcanic Processes.* (eds. K. D. Putirka and F. J., Tepley, III) Mineralogical Society of America and Geochemical Society, *Reviews in Mineralogy and Geochemistry* **69**, 445–478.

Blythe L.S., Deegan F.M., Freda C., Jolis E.M., Masotta M., Misiti V., Taddcucci J. and Troll V.R. (2015). CO_2 bubble generation and migration during magma-carbonate interaction. *Contrib. Mineral. Petrol.* **169**, 42.

Bohrson W.A., Spera F.J., Ghorso M.S., Brown G.A., Creamer J.B. and Mayfield A. (2014) Thermodynamic model for energy-constrained open-system evolution of crustal magma bodies undergoing simultaneous recharge, assimilation and crystallization: the Magma Chamber Simulator. *J. Petrol.* doi:10.1093/peyrology/egu036.

Borisova A.Y., Martel C., Pratomo I., Toutain J.-P., Sumarti S. and Surono (2011). "MERAPIDATA": New Petrologic and Geochemical Database of the Merapi Volcano, Central Java, Indonesia. *AGU Fall Meeting* (V21E-2536).

Borisova A.Y., Martel C., Gouy S., Pratomo I., Sumarti S., Toutain J.-P., Bindeman I.N., de Parseval Ph., Metaxian J-Ph. and Surono (2013) Highly explosive 2010 Merapi eruption : Evidence for shallow-level crustal assimilation and hybrid fluid. *J. Volcan. Geotherm. Res.* **261**, 193–208.

Borisova A.Y., Faure F., Deloule E., Grégoire M., Béjina F., de Parseval Ph. and Devidal J.-L. (2014) Lead isotope signatures of Kerguelen plume-derived olivine-hosted melt inclusions: Constraints on the ocean island basalt petrogenesis. *Lithos* **198–199**, 153–171, http://dx.doi.org/10.1016/j.lithos.2014.03.022.

Brearley A.J. and Jones R.H. (1998) Chondritic meteorites. In: Planetary Materials (ed. Papike J.J.). *Reviews in Mineralogy*, Mineralogical Society of America, **36**, 3-1 – 396.

Cashman K.V. (1993) Relationship between plagioclase crystallization and cooling rate in basaltic melts. *Contrib. Mineral. Petrol.* **113**, 126–142.

Chadwick J.P., Troll V.R., Ginibre C., Morgan D., Gertisser R., Waight T.E. and Davidson J.P. (2007) Carbonate assimilation at Merapi volcano, Java, Indonesia: insights from crystal isotope stratigraphy. *J. Petrol.* **48**, 1793–1812.

Chadwick J.P., Troll V.R., Waight T.E., van der Zwan F.M. and Schwarzkopf L.M. (2013) Petrology and geochemistry of igneous inclusions in recent Merapi deposits: a window into the sub-volcanic plumbing system. *Contrib. Mineral. Petrol.* **165**, 259–282.

Cherniak D. J. (2010). Cation diffusion in feldspars. In: Diffusion in minerals and melts, (eds. Y. Zhang and D.J. Cherniak) Reviews in Mineralogy and Geochemistry, 72, Mineralogical Society of America, Geochemical Society. 691-733.

Cooper K.M., Kent A.J.R. (2014). Rapid remobilization of magmatic crystals kept in cold storage. *Nature* **506**, 480-483.

Costa F., Andreastuti S., Bouvet de Maisonneuve C. and Pallister J. (2013) Petrological insights into the storage conditions, and magmatic processes that yielded the centennial 2010 Merapi explosive eruption. *J. Volcan. Geotherm. Res.* **261**, 209–235.

Davidson J.P., Morgan D.J., Charlier B.L.A. (2007). Isotopic microsapling of magmatic rocks. *Elements* **3**, 253–259.

Debaille V., Doucelance R., Weis D. and Schiano P. (2006) Multi-stage mixing in subduction zones: Application to Merapi volcano (Java island, Sunda arc). *Geochim. Cosmochim. Acta* **70,** 723–741.

Deegan F. M., Troll V. R., Freda C., Misiti V., Chadwick J. P., McLeod C. L. and Davidson J. P. (2010) Magma–carbonate interaction processes and associated CO_2 release at Merapi volcano, Indonesia: insights from experimental petrology. *J. Petrol.* **51**, 1027–1051.

Edwards B. R. and Russell J. K. (1998) Time scales of magmatic processes: New insights from dynamic models for magmatic assimilation. *Geology* **26**, 1103–1106.

Farver J. R. (2010). Oxygen and hydrogen diffusion in minerals. In: Diffusion in minerals and melts, (eds. Y. Zhang and D.J. Cherniak) Reviews in Mineralogy and Geochemistry, 72, Mineralogical Society of America, Geochemical Society. 447-507.

Eiler J. M., Schiano P., Kitchen N. and Stolper E. M. (2000) Oxygen-isotope evidence for recycled crust in the sources of mid-ocean-ridge basalts. *Nature* **403**, 530–534.

Elphick S.C., Graham C.M. and Dennis P.F. (1988) An ion microprobe study of anhydrous oxygen diffusion in anorthite: A comparison with hydrothermal data and some geological implications. *Contrib. Mineral. Petrol* **100**, 490–495.

Erdmann S., Martel C., Pichavant M., Bourdier J.-L., Champallier R., Komorowski J.-C., Noer C. (2016) Constraints from phase equilibrium experiments on pre-eruptive storage conditions in mixed magma systems: a case study on crystal-rich basaltic andesites from Mount Merapi, Indonesia. *J. Petrol.,* **57**, 535-560.

Erdmann S., Scaillet B. and Kellett D.A. (2012) Textures of peritectic crystals as guides to reactive minerals in magmatic systems: new insights from melting experiments. *J. Petrol.,* **53**, 2231-2258, doi: 10.1093/petrology/egs048.

Farver J.R. (2010) Oxygen and hydrogen diffusion in minerals. In: *Diffusion in minerals and melts.* (eds. Y. Zhang and D.J. Cherniak), *Reviews in Mineralogy and Geochemistry* **72**, Mineralogical Society of America, Geochemical Society, 447–490.

Feig S.T., Koepke J. and Snow J.E. (2006) Effect of water on tholeiitic basalt phase equilibria: an experimental study under oxidizing conditions. *Contrib. Mineral. Petrol.* **152**, 611–638.

Freda C., Gaeta M., Misiti V., Mollo S., Dolfi D. and Scarlato P. (2008) Magma–carbonate interaction: an experimental study on ultrapotassic rocks from Alban Hills (Central Italy). *Lithos* **101**, 397–415.

Gaeta M., Di Rocco T. and Freda C. (2009) Carbonate Assimilation in Open Magmatic Systems: the Role of Melt-bearing Skarns and Cumulate-forming Processes. *J. Petrol.*, **50**, 361-385, doi:10.1093/petrology/egp002.

Gardner M.F., Troll V.R., Gamble J.A., Gertisser R., Hart G.L., Ellam R.M., Harris C. and Wolff J.A. (2013) Crustal differentiation processes at Krakatau volcano, Indonesia. *J. Petrol.* **54**, 149–182.

Gertisser R. and Keller J. (2003) Temporal variations in magma composition at Merapi Volcano (Central Java, Indonesia): magmatic cycles during the past 2000 years of explosive activity. *J. Volcan. Geotherm. Res.* **123**, 1–23.

Gurenko A.A., Chaussidon M. and Schmincke H.-U. (2001) Magma ascent and contamination beneath one intraplate volcano: Evidence from S and O isotopes in glass inclusions and their host clinopyroxenes from Miocene basaltic hyaloclastites southwest of Gran Canaria (Canary Islands). *Geochim. Cosmochim. Acta* **65**, 4359–4374.

Gurenko A.A., Bindeman I.N., Sigurdsson I.A. (2015) To the origin of Icelandic rhyolites: insights from partially melted leucocratic xenoliths. *Contrib. Mineral. Petrol.* DOI: 10.1007/s00410-015-1145-4.

Handley H.K., Macpherson C.G. and Davidson J.P. (2010) Geochemical and Sr-O isotopic constraints on magmatic differentiation at Gede Volcanic Complex, West Java, Indonesia. *Contrib. Mineral. Petrol.* **159**, 885–908.

Handley H.K., Blichert-Toft J., Gertisser R., Macpherson C.G., Turner S.P., Zaennudin A., and Abdurrachman M. (2014) Insights from Pb and O isotopes into along-arc variations in subduction inputs and crustal assimilation for volcanic rocks in Java, Sunda arc, Indonesia. *Geochim. Cosmochim. Acta* **139**, 205–226.

Harmon R.S., Gerbe M.-C. (1992) The 1982-83 eruption at Galunggung volcano, Java (Indonesia): Oxygen isotope geochemistry of a chemically zoned magma chamber. *J. Petrol* **33**, 585–609.

Harris C., Ashwal L.D. (2002). The origin of low $\delta^{18}O$ granites and related rocks from the Seychelles. *Contrib. Mineral. Petrol.* **143**, 366–376.

Iacono-Marziano G., Gaillard F. and Pichavant M. (2008) Limestone assimilation by basaltic magmas: an experimental re-assessment and application to Italian volcanoes. *Contrib. Mineral. Petrol.* **155**, 719–738.

Iacono-Marziano G., Gaillard F., Scaillet B., Pichavant M. and Chiodini G. (2009) Role of non-mantle CO_2 in the dynamics of volcano degassing: the Mount Vesuvius example. *Geology* **37**, 319–322.

Jacques G., Hoernle K., Gill J., Hauff F., Wehrmann H., Garbe-Schonberg D., van der Bogaard P., Bindeman I. and Lara L.E. (2013) Across-arc geochemical variations in the Southern Volcanic Zone, Chile (34.5 – 38.0 degrees S): Constraints on mantle wedge and slab input compositions. *Geochim. Cosmochim. Acta* **123**, 218–243.

Jamshidi K., Ghasemi H., Troll V.R., Sadeghian M. and Dahren B. (2015). Magma storage and plumbing of adakite-type post-ophiolite intrusions in the Sabzevar ophiolitic zone, northeast Iran. *Solid Earth* **6**, 49–72.

Jarosevich E., Nelen J.A. and Norberg J.A. (1980) Reference samples for electron microprobe analysis. *Geostand. Newslett.* **4**, 257–258.

Jeffery A.J., Gertisser R., Troll V.R., Jolis E.M., Dahren B., Harris C., Tindle A.G., Preece K., O'Driscoll B., Humaida H. and Chadwick J.P. (2013) The pre-eruptive magma plumbing system of the 2007 – 2008 dome-forming eruption of Kelut volcano, East Java, Indonesia. *Contrib. Mineral. Petrol.* doi: 10.1007/s00410-013-0875-4.

Jochum, K.P., Stoll, B., Herwig, K., Willbold, M., Hofmann, A.W., Amini, M., Aarburg, S., Abouchami, W., Hellebrand, E., Mocek, B., Raczek, I., Stracke, A., Alard, O., Bouman, C., Becker, S., Dücking, M., Brätz, H., Klemd, R., de Bruin, D., Canil, D., Cornell, D., de Hoog, C.-J., Dalpé, C., Danyushevsky, L., Eisenhauer, A., Gao, Y., Snow, J.E., Groschopf, N., Günther, D., Latkoczy, C., Guillong, M., Hauri, E.H., Höfer, H.E., Lahaye, Y., Horz, K., Jacob, D.E., Kasemann, S.A., Kent, A.J.R., Ludwig, T., Zack, T., Mason, P.R.D., Meixner, A., Rosner, M., Misawa, K., Nash, B.P., Pfänder, J., Premo, W.R., Sun,W.D., Tiepolo, M., Vannucci, R., Vennemann, T., Wayne, D., Woodhead, J.D., 2006. MPI-DING reference glasses for in situ

microanalysis: new reference values for element concentrations and isotope ratios. *Geochemistry, Geophysics, Geosystems* 7 (2). http://dx.doi.org/10.1029/2005GC001060.

Jolis E. M., Freda C., Troll V. R., Deegan F. M., Blythe L. S., McLeod C. L. and Davidson J. P. (2013) Experimental simulation of magma–carbonate interaction beneath Mt. Vesuvius, Italy. *Contrib. Mineral. Petrol.* doi: 10.1007/s00410-013-0931-0.

Kirkpatrick R.J. (1981) Kinetics of crystallization of igneous rocks. In: *Kinetics of geochemical processes.* (eds. Lasaga A.C. and Kirkpatrick R.J.) *Reviews in Mineralogy*, **8**, Mineralogical Society of America.

Kita N.T., Ushikubo T., Fu B. and Valley J.W. (2009) High precision SIMS oxygen isotope analysis and the effect of sample topography. *Chem. Geol.* **264**, 43–57.

Lange A.E., Nielsen R.L., Tepley F.J., III, Kent A.J.R. (2013). Diverse Sr isotope signatures preserved in mid-oceanic-ridge basalt plagioclase. *Geology* **41**, 279-282.

Lasaga A. C. (1998) *Kinetic Theory in the Earth Sciences*. Princeton Series in Geochemistry. Princeton, Chichester: Princeton University Press.

Lofgren G.E., Williams R.J., Donaldson C.H., and Usselman T.M. (1975) An experimental investigation of porphyritic texture. *Geol. Soc. Am. Abstr. Progr.* **7**, 1173–1174.

Martin E., Bindeman I. and Grove T.L. (2011) The origin of high-Mg magmas in Mt. Shasta and Medicine Lake volcanoes, Cascade Arc (California): higher and lower than mantle oxygen isotope signatures attributed to current and past subduction. C*ontrib. Mineral. Petrol.* **162**, 945–960.

Martel C., Radadi Ali A., Poussineau S., Gourgaud A. and Pichavant M. (2006) Basalt inherited microlites in silicic magmas: evidence from Mt. Pelée (Martinique, F.W.I.). *Geology* **34**, 905–908.

Minarik W.G. (1998) Complications to carbonate melt mobility due to the presence of an immiscible silicate melt. *J. Petrol.* **39**, 1965–1973.

Mollard E., Martel C. and Bourdier J.-L. (2012) Decompression-induced crystallization in hydrated silica-rich melts: empirical models of experimental plagioclase nucleation and growth kinetics. *J. Petrol.* **53**, 1743–1766.

Mollo S., Gaeta M., Freda C., DiRocco T., Misiti V., Scarlato P. (2010) Carbonate assimilation in magmas: a reappraisal based on experimental petrology. *Lithos* **114**, 503–514.

Papike J.J., Ryder G., Shearer C.K. (1998) Lunar samples. In: Planetary Materials (ed. Papike J.J.). *Reviews in Mineralogy*, Mineralogical Society of America, **36**, 5-1 – 188.

Pichavant M., Martel C., Bourdier J.-L. and Scaillet B. (2002) Physical conditions, structure, and dynamics of a zoned magma chamber: Mount Pelée (Martinique, Lesser Antilles Arc). *J. Geophys. Res.* **107** (B5) (10.1029).

Plechov P., Shishkina T.A., Ermakov V.A. and Portnyagin M.V. (2008) Formation conditions of allivalites, olivine-anorthite crystal enclaves, in the volcanics of the Kuril-Kamchatka arc. *Petrology* **16**, 232–260.

Preece K., Gertisser R., Barclay J., Berlo K., Herd R.A., Edinburgh Ion Microprobe Facility (2014). Pre- and syn-eruptive degassing and crystallisation processes of the 2010 and 2006 eruptions of Merapi volcano, Indonesia. *Contrib Mineral Petrol*, **168**, 1061. DOI 10.1007/s00410-014-1061-z.

Prouteau G. and Scaillet B. (2003) Experimental Constraints on the Origin of the 1991 Pinatubo Dacite, *J. Petrol.* **44**, 2203–2241.

Python M., Ceuleneer G., Ishida Y., Barrat J.-A. and Arai S. (2007) Oman diopsidites: a new lithology diagnostic of very high temperature hydrothermal circulation in mantle peridotite below oceanic spreading centres. *Earth Planet. Sci. Lett.* **255**, 289–305.

Reubi O., Blundy J. (2009) A dearth of intermediate melts at subduction zone volcanoes and the petrogenesis of arc andesites. *Nature*, **461**, 1269-U103.

Sato K., Kashima K. and Sunagawa I. (1981) Measurements of nucleation rates and real growth rates of plagioclase in a solution of basaltic composition. *J. Japan. Assoc. Min. Petr. Econ. Geol.* **76**, 294–307.

Singer B.S., Pearce T.H., Kolisnik A.M., Myers J.D. (1993). Plagioclase zoning in mid-Pleistocene lavas from the Seguam volcanic center, central Aleutian arc, Alaska. *American Mineralogist* **78**, 143-157.

Sisson T.W. and Grove T.L. (1993). Experimental investigation of the role of H_2O in calc-alkaline differentiation and subduction zone magmatism. *Contrib. Mineral. Petrol.* 113, 143-166.

Surono, Jousset P., Pallister J., Boichu M., Buongiorno M.F., Budisantoso A., Costa F., Andreastuti S., Prata F., Schneider D., Clarisse L., Humaida H., Sumarti S., Bingnami C., Griswold J., Carn S., Oppenheimer C. and Lavigne F. (2012) The 2010 explosive eruption of Java's Merapi volcano — a "100-year" event. *J. Volcanol. Geotherm. Res.* **241–242**, 121–135.

Suzuki K., Kitajima K., Sawaki Y., Hattori K., Hirata T., Maruyama S. (2015). Ancient oceanic crust in island arc lower crust: Evidence from oxygen isotopes in zircons from the Tanzawa Tonalitic Pluton. *Lithos* **228-229**, 43-54.

Taylor S.R. and McLennan S.M. (1985). *The Continental Crust: Its Composition and Evolution*. Blackwell Scientific Publications.

Troll V.R., Deegan F.M., Jolis E.M., Harris C., Chadwick J.P., Gertisser R., Schwarzkopf L.M., Borisova A.Y., Bindeman I.N., Sumarti S. and Preece K. (2013). Magmatic differentiation processes at Merapi Volcano: inclusion petrology and oxygen isotopes. *J. Volcanol. Geotherm. Res.* **261**, 38–49.

Troll V.R., Hilton D.R., Jolis E.M., Chadwick J.P., Blythe L.S., Deegan F.M., Schwarzkopf L.M., and Zimmer M. (2012). Crustal CO_2 liberation during the 2006 eruption and earthquake events at Merapi volcano, Indonesia. *Geophys. Res. Lett.* **39**, L11302.

Valley J.W., Kitchen N., Kohn M.J., Niendorf C.R. and Spicuzza M.J. (1995). UWG-2, a garnet standard for oxygen isotope ratios: Strategies for high precision and accuracy with laser heating. *Geochim. Cosmichim. Acta* **59**, 5223–5231.

Valley J.W. and Kita N.T. (2009) In situ oxygen isotope geochemistry by ion microprobe. *Mineraligical Association of Canada Short Course*, **41**, 19–63.

van der Zwan F.M., Chadwick J.P. and Troll V.R. (2013) Textural history of recent basaltic-andesites and plutonic inclusions from Merapi volcano. *Contrib. Mineral. Petrol.* **166**, 43–63.

Winpenny B. and Maclennan J. (2014) Short length scale oxygen isotope heterogeneity in the Icelandic mantle: Evidence from plagioclase compositional zones. *J. Petrol.* **55**, 2537–2566.

Zhang Y. and Cherniak D.J. (2010) Diffusion in minerals and melts: Introduction. In: *Diffusion in Minerals and Melts.* (eds. Zhang Y. and Cherniak D.J.) *Reviews in Mineralogy and Geochemistry.* **72**, Mineralogical Society of America, Geochemical Society, 1–3.

Zhao, Z. F. and Zheng, Y. F. (2003) Calculation of oxygen isotope fractionation in magmatic rocks. *Chem. Geol.* **193**, 59–80.

Zheng, Y.F. (1993) Calculation of oxygen isotope fractionation in anhydrous silicate minerals. *Geochim. Cosmochim. Acta* **57**, 1079-1091.

Table 1. Instrumental mass fractionation (IMF, $\Delta^{18}O_{IMF}$) for oxygen isotopes in the first analytical session

Reference plagioclase	№[a]	An[b] mol.%	$\delta^{18}O_{SIMS}$[c] ‰	$1\sigma_{repr.}$[d] ‰	$\delta^{18}O_{LF}$[e] ‰	IMF[f] ‰	IMF[g] ‰
M2010GR-a AB data subset							
Std 1	18	0.32	-2.64	0.05	11.01	-13.65	-13.59
Std 2	18	23.56	-6.00	0.27	6.82	-12.82	-12.81
Std 3	18	61.09	-4.18	0.08	6.76	-10.94	-10.93
Std 5	14	55.03	-4.26	0.30	7.00	-11.26	-11.24
M2010PF-a AB data subset							
Std 1	8	0.32	-2.34	0.19	11.01	-13.36	-13.30
Std 2	9	23.56	-5.69	0.12	6.82	-12.51	-12.50
Std 3	13	61.09	-3.94	0.15	6.76	-10.70	-10.68
Std 5	10	55.03	-4.33	0.04	7.00	-11.33	-11.32
M2010PF-b1 AB data subset							
Std 1	9	0.32	-2.49	0.06	11.01	-13.51	-13.45
Std 2	9	23.56	-5.79	0.10	6.82	-12.61	-12.60
Std 3	9	61.09	-4.09	0.02	6.76	-10.84	-10.83
Std 5	4	55.03	-4.26	0.07	7.00	-11.25	-11.24

[a] № = number of replicates;

[b] anorthite content given in mol.%;

[c] Averaged results of the replicate measurements of reference plagioclases by SIMS;

[d] $1\sigma_{repr} = 1\sigma$ S.D. calculated from the replicative measurements of $\delta^{18}O_{SIMS}$;

[e] Averaged results of the replicate measurements of reference plagioclases by laser fluorination;

[f] IMF ($\Delta^{18}O_{IMF(RM)}$), instrumental mass fractionation calculated from Eqn. 1;

[g] Instrumental mass fractionation (IMF, $\Delta^{18}O_{IMF}$) calculated from Eqn. 3.

Table 2. Oxygen isotope data on the 1994 – 1998 Merapi calc-silicate xenoliths

Year of the Merapi eruption	Sample number	Mineral assemblage*	$\delta^{18}O_{SMOW}$** values in per mil, ‰	SiO_2 (average) wt.% according to EDS analyses by SEM
1994	M-94-CS-104 crystal (1)	Woll	11.39	50
1994	M-94-CS-106 crystal (1)	major Woll	11.03	49
1994	M-94-CS-106 crystal (2)	major Grs	10.21	39
1994	M-94-CS-106 crystal (3)	Woll+An+Glass	8.70	59
1994	M-94-CS-106 crystal (4)	Woll+Grs	9.62	45
1998	M-XCS-1 crystal (1)	Woll	12.43	50
1998	M-XCS-1 crystal (1a)	Woll ± Calc	17.22	50
1998	M-XCS-4 dark crystal (1)	major TiMgt	6.53	0.0

* The following abbreviations have been used: "An" = anorthite; "Calc" = calcite; "Glass" = silicate glass; "Grs" = grossular; "TiMgt oxide" = titanomagnetite; "Woll" = wollastonite; "major" means predominant phase. EDS analyses by SEM (see details in the section 3.2).

** The values are obtained by laser fluorination at the University of Oregon (USA).

Table 3. Composition of glass inclusions in M2010GR-a plagioclase

Composition:	SiO_2	TiO_2	Al_2O_3	FeO	MgO	MnO	CaO	Na_2O	K_2O	P_2O_5	SO_2	Cl	Total	CaO/Na_2O	CaO/Al_2O_3	An_{host} min*	An_{host} max
Units :	wt.%															mol. %	
8 / 68 / Point 113	58.3	1.16	12.8	6.39	2.07	0.26	2.28	2.58	3.65	0.46	0.04	1.05	91.0	0.88	0.18	82	82
8 / 69 / Point 114	59.7	0.38	21.8	2.10	0.53	0.07	5.70	5.71	3.21	0.09	0.03	0.21	99.5	1.00	0.26	82	82
8 / 100 / Point 145	63.7	0.84	16.4	4.33	1.00	0.27	2.62	2.68	4.46	0.16	0.03	0.53	97.0	0.98	0.16	91	92
8 / 101 / Point 146	64.8	0.73	14.8	4.90	1.12	0.12	1.83	2.56	4.95	0.17	0.01	0.57	96.5	0.71	0.12	91	92

*"min" and "max" – minimal and maximal anorthite contents (An_{host}) in the host plagioclase.

Table 4. Partitioning coefficients between plagioclase and melts and the calculated composition of the 2010 Merapi melts

An mol.%	Ln (K_d^{Fe})	K_d^{Fe*}	Reference	FeO_{Plag}, wt.%	FeO_{melt}, wt.%
	Experimental data			Natural data on the Merapi	Model for the Merapi
95	-2.5	0.08	Bindeman et al. 1998	0.8	10
90	-2.4	0.09		0.8	9
80	-2.2	0.11		0.8	7
95	-2.5	0.08	Bindeman et al. 1998	0.2	3
90	-2.4	0.09		0.2	2
80	-2.2	0.11		0.2	2
89	-	0.11	Pichavant et al. 2002	0.8	7
88	-	0.14		0.8	6
86	-	0.11		0.8	7
89	-	0.11	Pichavant et al. 2002	0.2	2
88	-	0.14		0.2	1.4
86	-	0.11		0.2	2
An mol.%		$K_d^{CaO/Na2O*}$	Reference	CaO/Na_2O_{Plag}	CaO/Na_2O_{melt}
	Experimental data			Natural data on the Merapi	Model for the Merapi
95		3 – 4	Martel et al. 2006	34	9 – 11
90		3 – 4		16	4 – 5

An mol.% is anorthite content in plagioclase.

*K_d^{Fe} and $K_d^{CaO/Na2O}$, partition coefficients are calculated according Bindeman et al. (1998), Pichavant et al. (2002) and Martel et al. (2006).

FeO_{Plag}, and FeO_{melt} wt.% are FeO contents in plagioclase and melt, respectively.

CaO/Na_2O_{Plag} and CaO/Na_2O_{melt} are CaO/Na_2O ratios in plagioclases and melts, respectively.

Table 5. Calculation of timescales based on ^{18}O diffusion in anorthite

Temperature	Scale		Diffusion coefficient	Zonation timescale	
			Elphick et al. (1988)**	Crank (1975)***	
T	2 h*		D^T	t at $C/C_o = 0.4$	
(°C)	(μm)	(m)	(m^2/s)	(s)	(yr)
1100	50	5.00E-5	1.05E-18	10.81E+08	34

* - data from Figs. 3 – 5. The suggested scale 2h is equal to 50 μm.

** - D^T data from Elphick et al. (1988), where D°(m^2/s) =1.00E-09 and Q (kJ/mol) = 236.

*** - see equation (2.15) of Crank (1975) at conditions where x = h, $C/C_o = 0.4$.

Figure 1

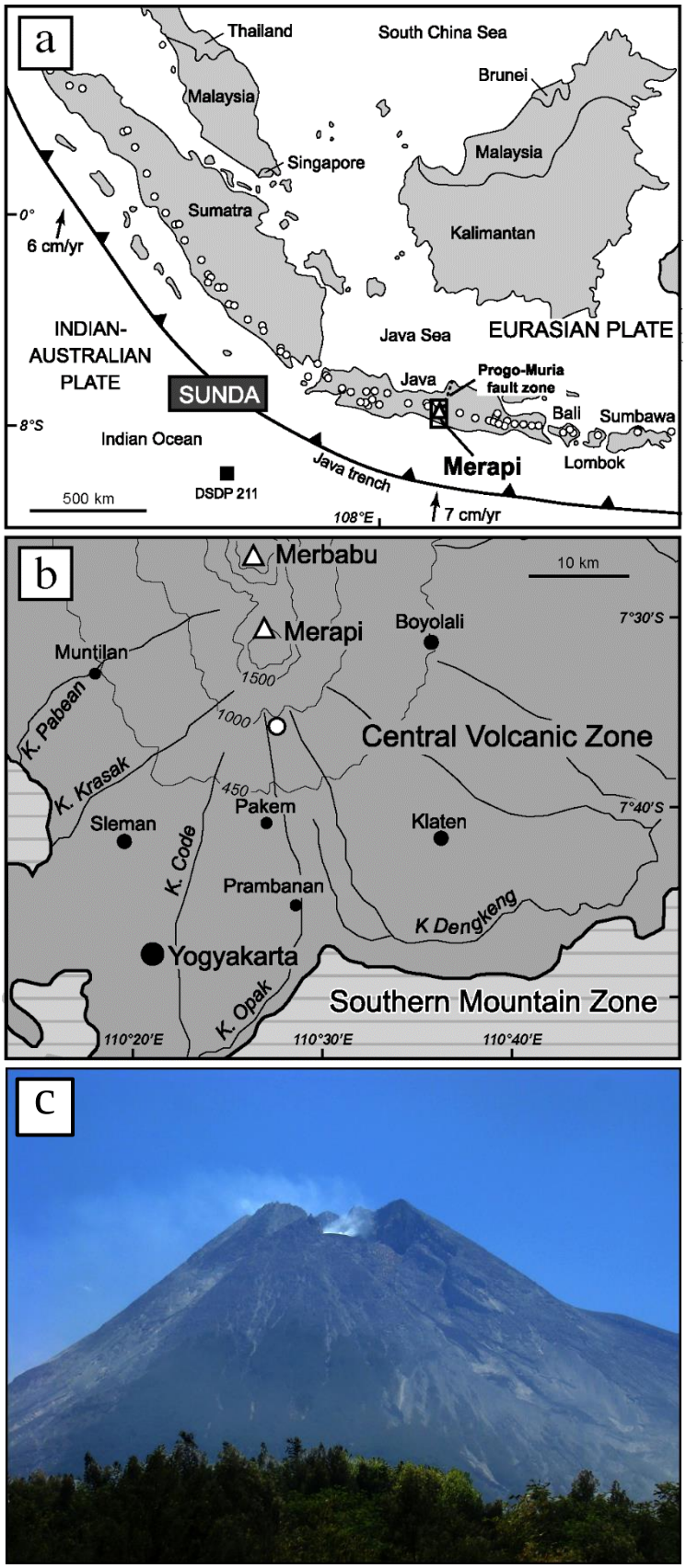

Figure 1

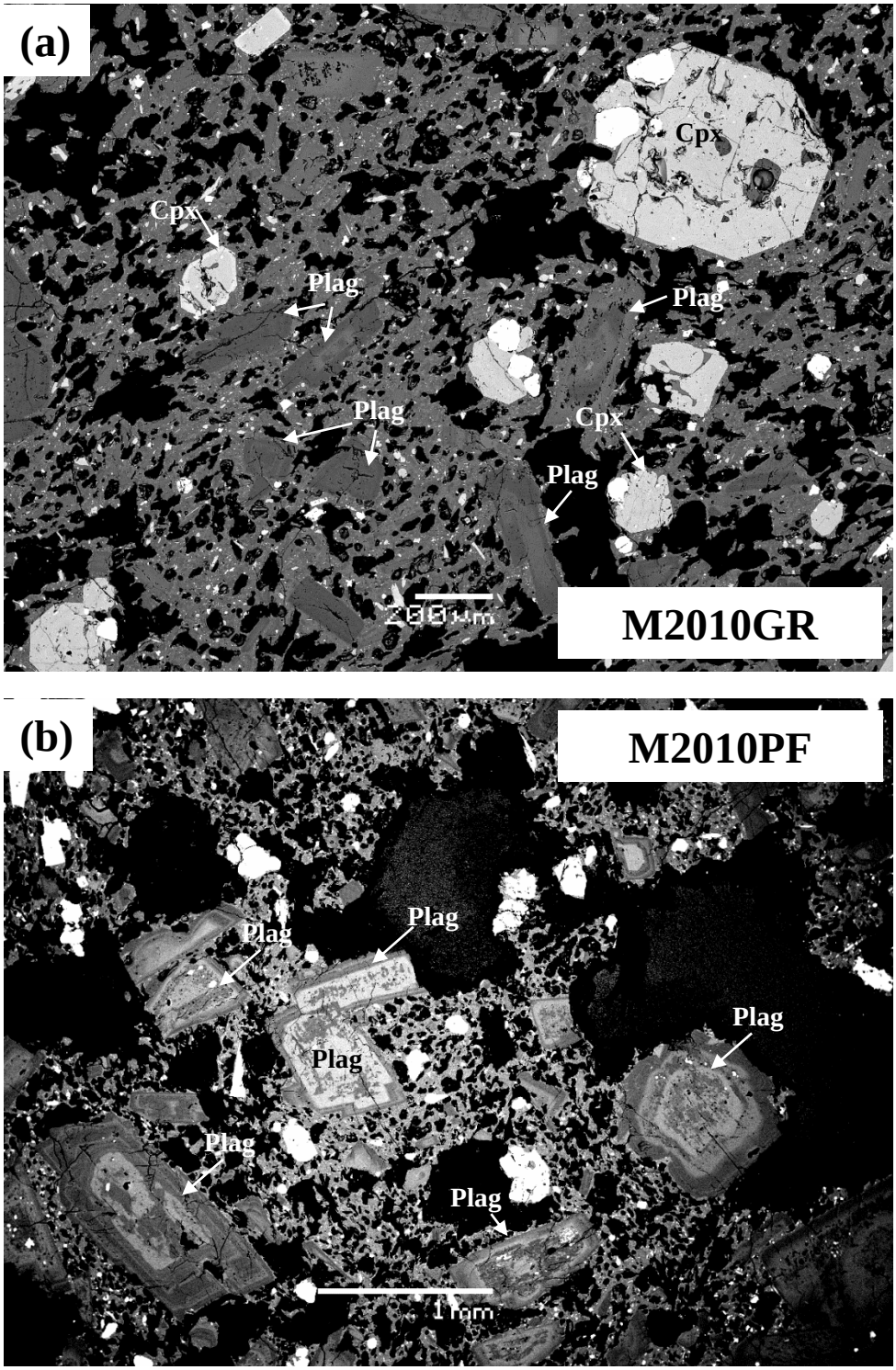
(a)
Cpx
Cpx
Plag
Plag
Plag
Cpx
Plag
200μm
M2010GR
(b)
M2010PF
Plag
Plag
Plag
Plag
Plag
Plag
1mm

Figure 2

Figure 3

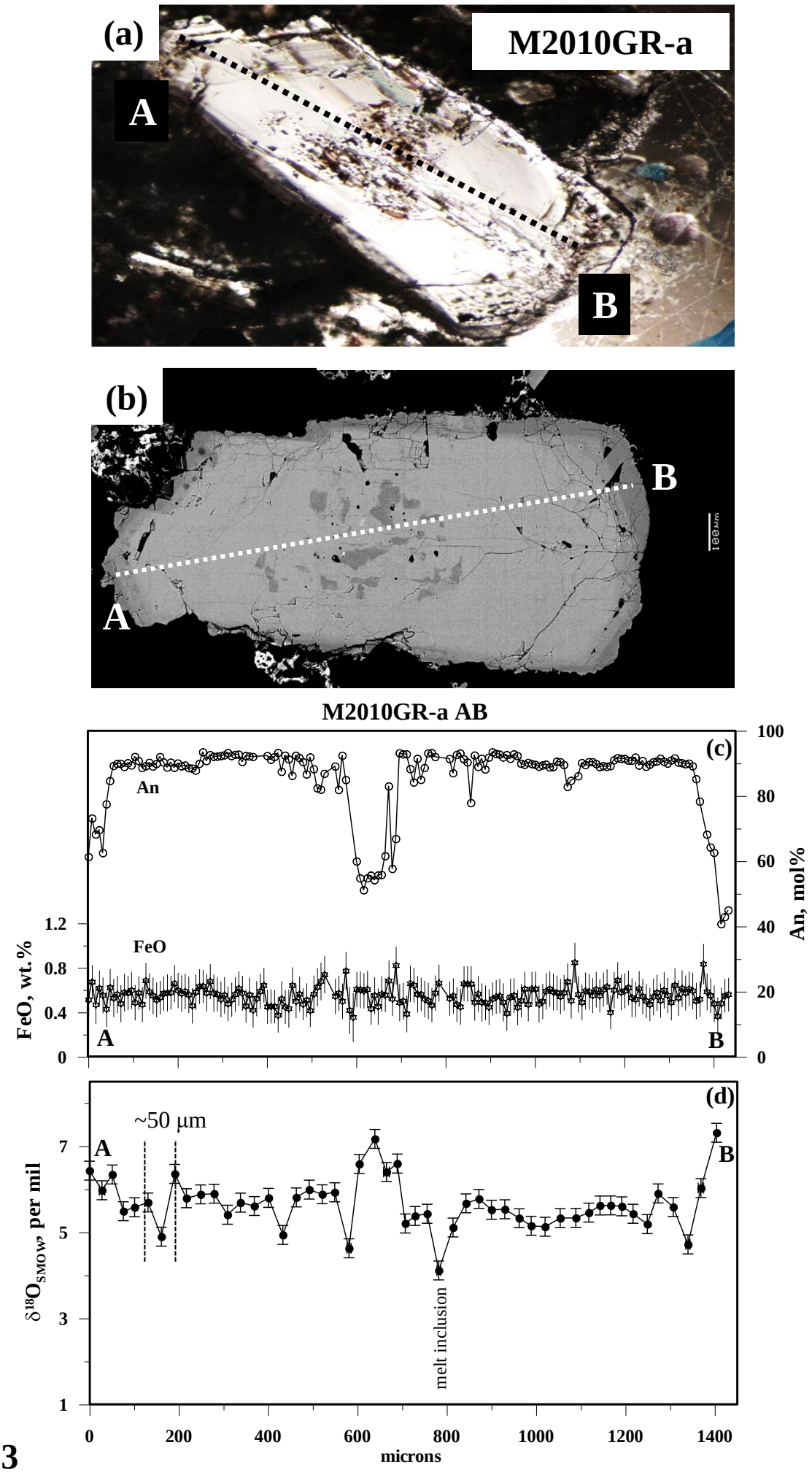

Figure 3

Figure 4

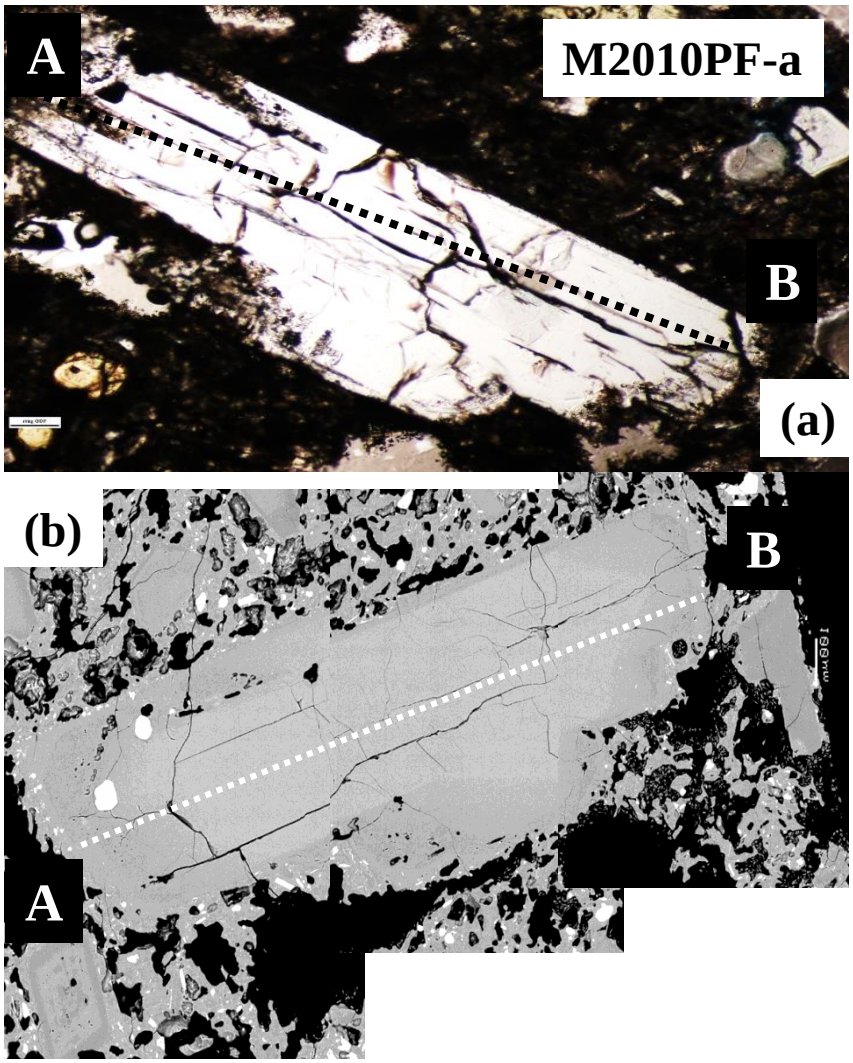

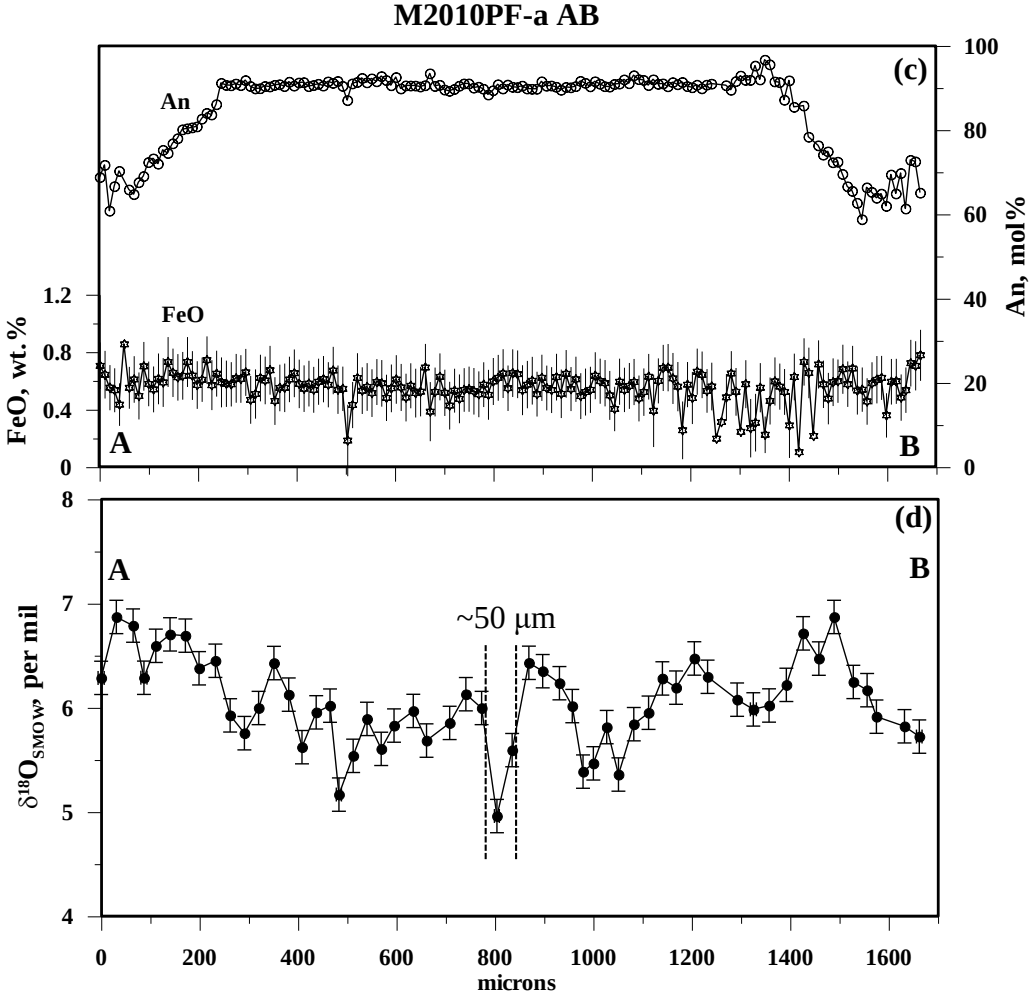

Figure 4

Figure 5

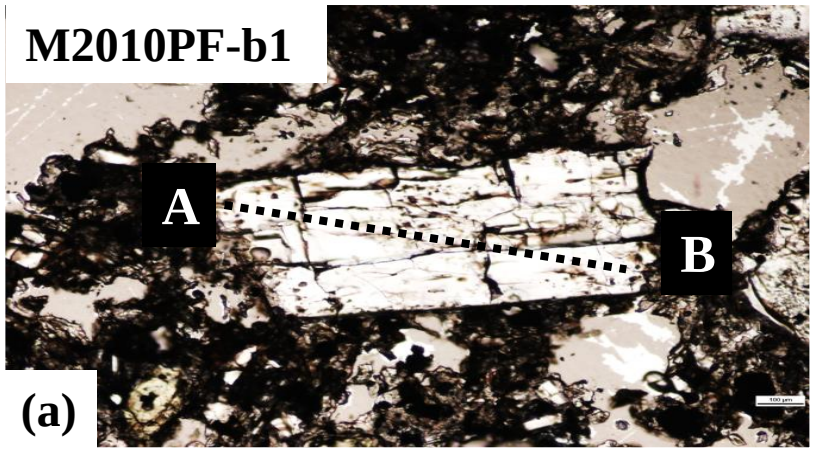

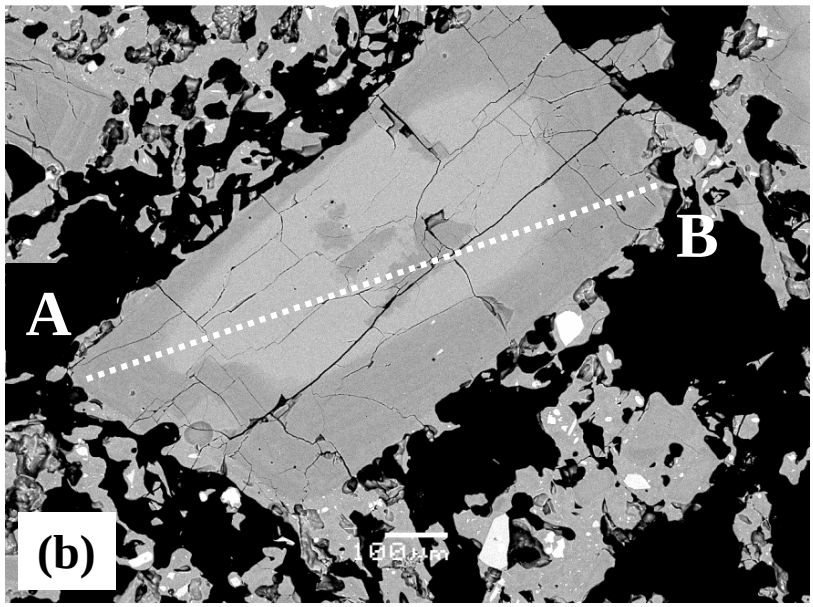

M2010PF-b1 AB

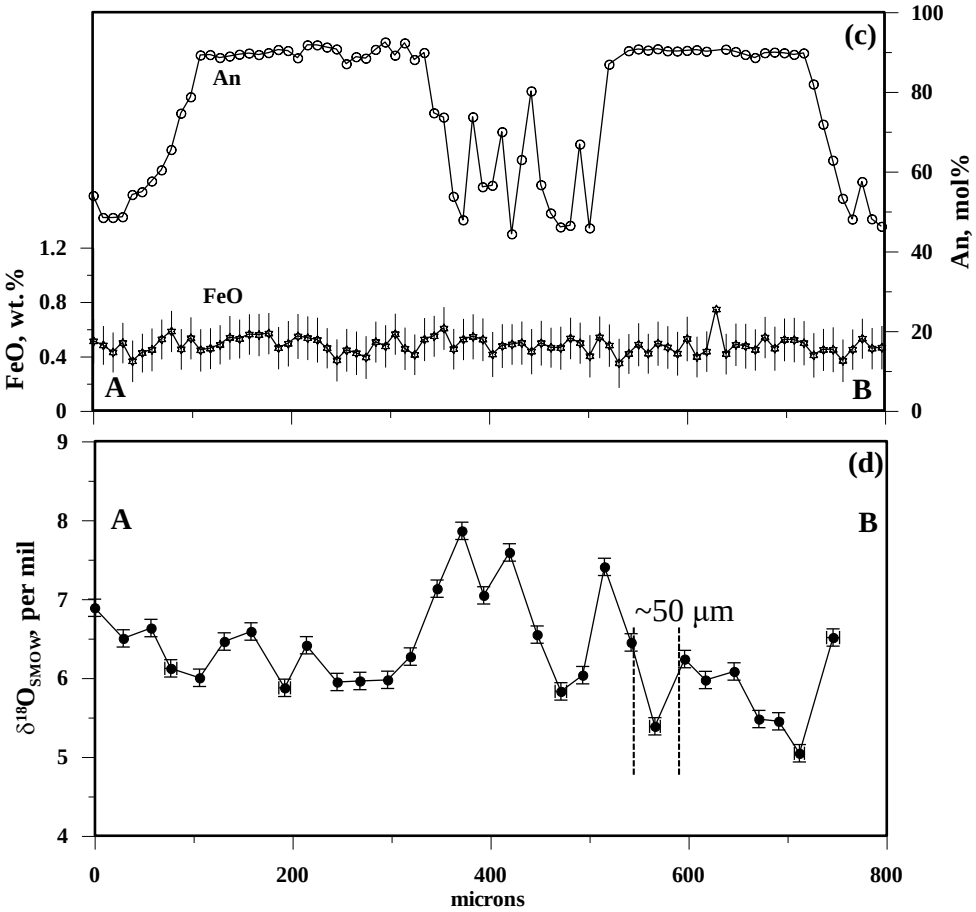

Figure 5

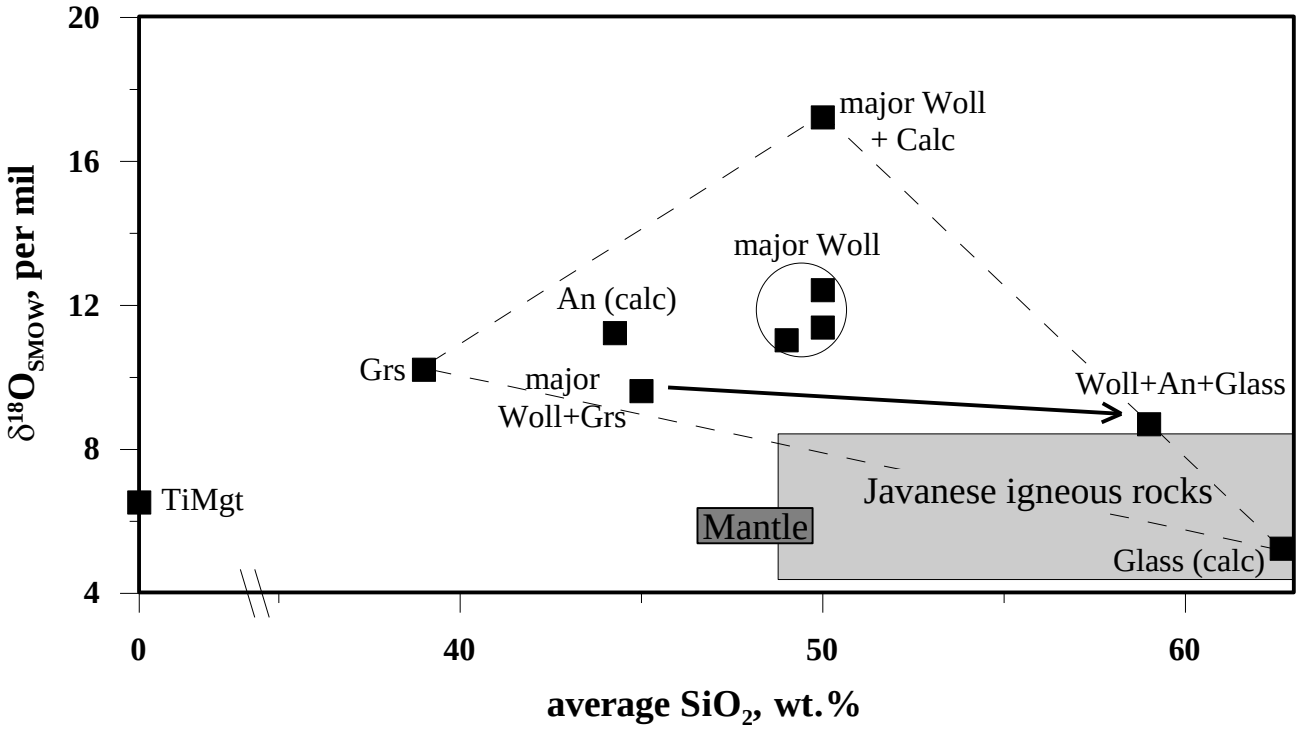
20
16
12
8
4
0
40
50
60
δ18OSMOW, per mil
average SiO2, wt.%
major Woll
+ Calc
major Woll
An (calc)
Grs
major
Woll+Grs
Woll+An+Glass
TiMgt
Javanese igneous rocks
Mantle
Glass (calc)

Figure 6

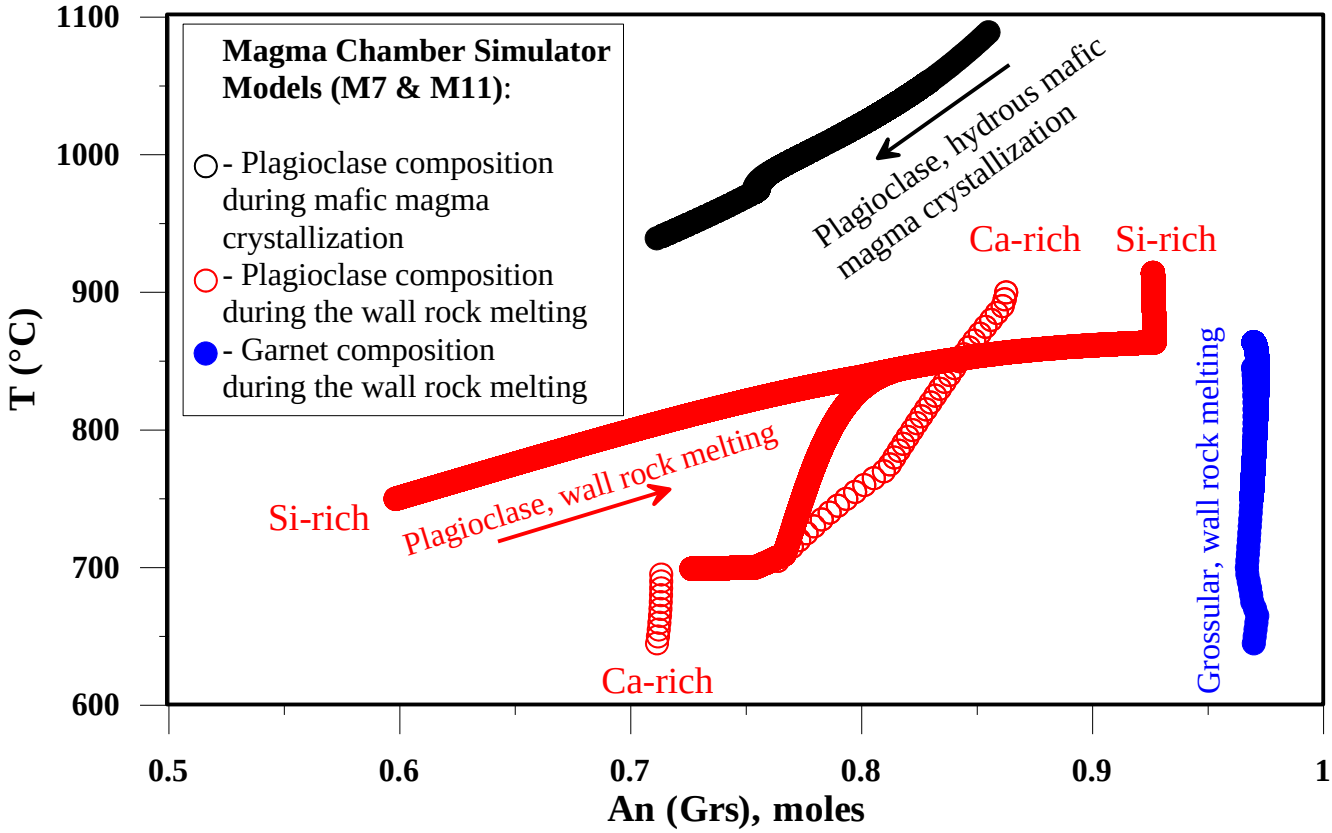
Magma Chamber Simulator Models (M7 & M11):
- Plagioclase composition during mafic magma crystallization
- Plagioclase composition during the wall rock melting
- Garnet composition during the wall rock melting
Plagioclase, hydrous mafic magma crystallization
Ca-rich
Si-rich
Si-rich
Plagioclase, wall rock melting
Ca-rich
Grossular, wall rock melting
T (°C)
1100
1000
900
800
700
600
0.5
0.6
0.7
0.8
0.9
1
An (Grs), moles

Figure 7

Figure 8

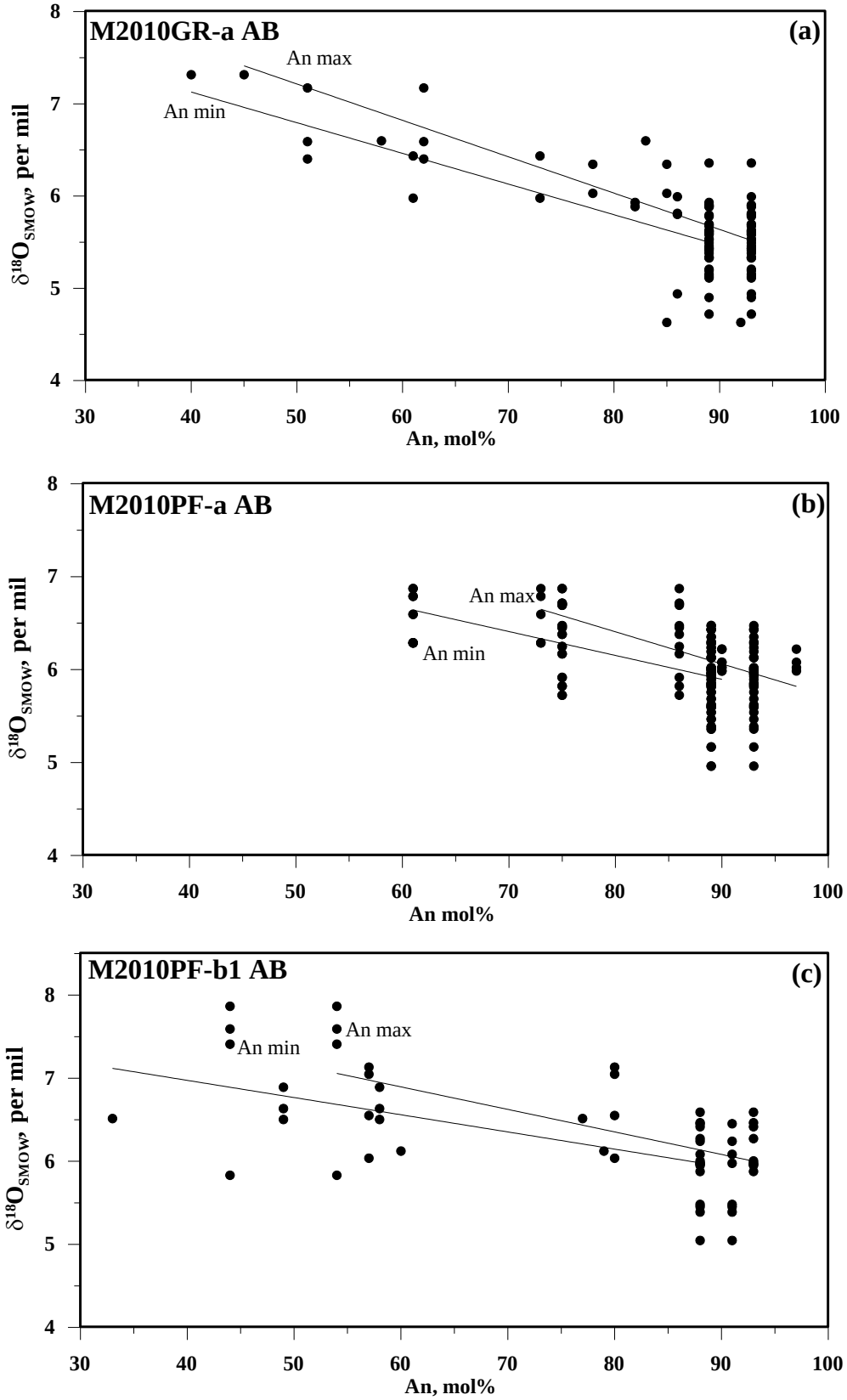

Figure 8

Figure 9

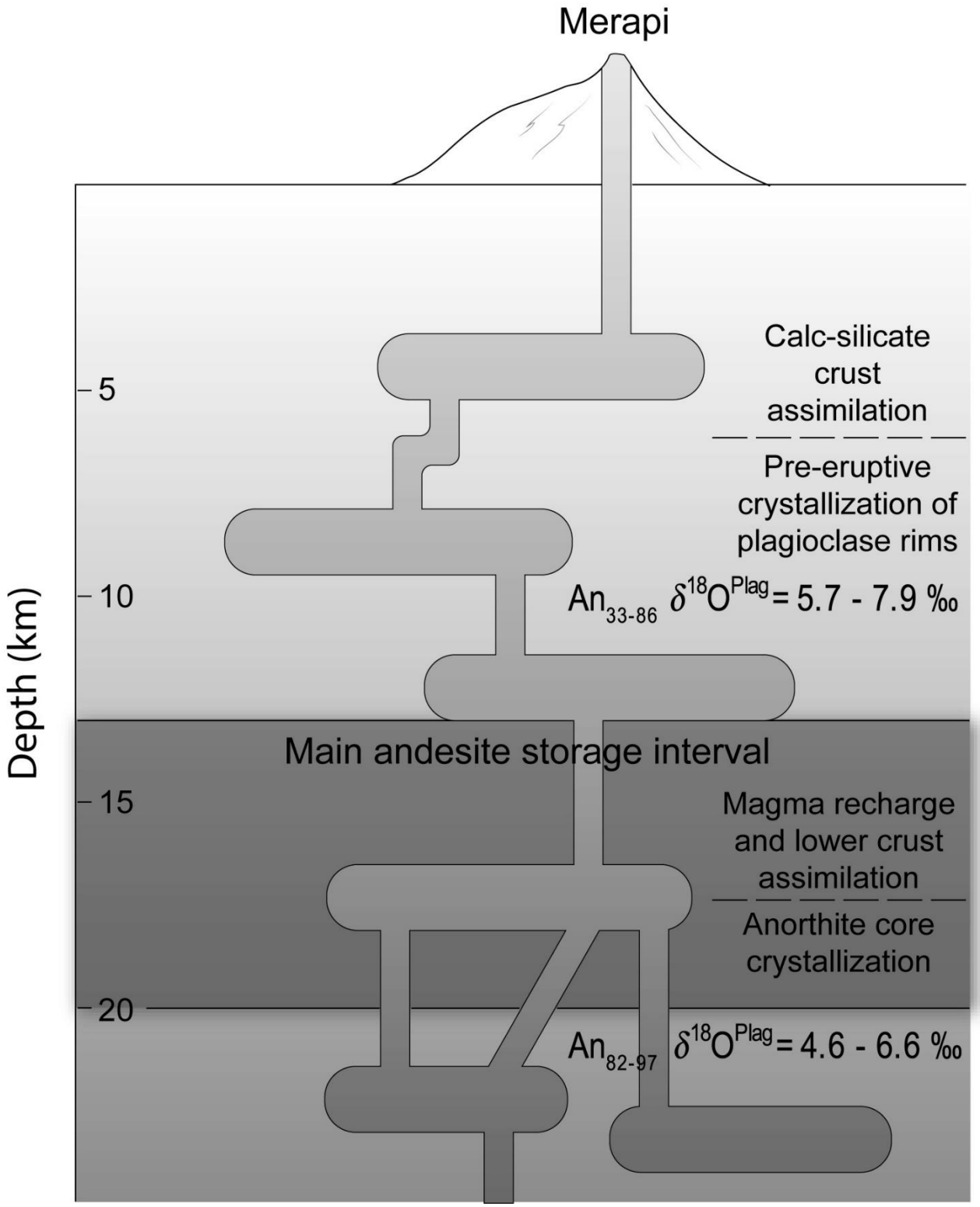

Figure 9